Struct Multidisc Optim (2016) 53:773–799
DOI 10.1007/s00158-015-1296-y

RESEARCH PAPER

Structural topology optimization under constraints on instantaneous failure probability

Junho Chun[1] · **Junho Song**[2] · **Glaucio H. Paulino**[3]

Received: 27 September 2014 / Revised: 12 May 2015 / Accepted: 17 June 2015 / Published online: 20 November 2015

Abstract Accurate prediction of stochastic responses of a structure caused by natural hazards or operations of non-structural components is crucial to achieve an effective design. In this regard, it is of great significance to incorporate the impact of uncertainty into topology optimization of structures under constraints on their stochastic responses. Despite recent technological advances, the theoretical framework remains inadequate to overcome computational challenges of incorporating stochastic responses to topology optimization. Thus, this paper presents a theoretical framework that integrates random vibration theories with topology optimization using a discrete representation of stochastic excitations. This paper also discusses the development of parameter sensitivity of dynamic responses in order to enable the use of efficient gradient-based optimization algorithms. The proposed topology optimization framework and sensitivity method enable efficient topology optimization of structures under stochastic excitations, which is successfully demonstrated by numerical examples of structures under stochastic ground motion excitations.

✉ Glaucio H. Paulino
paulino@gatech.edu

Junho Chun
jchun8@illinois.edu

Junho Song
junhosong@snu.ac.kr

[1] Department of Civil and Environmental Engineering, University of Illinois, Urbana, IL 61801, USA

[2] Department of Civil and Environmental Engineering, Seoul National University, Seoul 151-742, Republic of Korea

[3] School of Civil and Environmental Engineering, Georgia Institute of Technology, Atlanta, GA 30332, USA

Keywords Topology optimization · Stochastic excitation · Reliability based design optimization · Parameter sensitivity · Discrete representation

Nomenclature

$f(t)$	Stationary Gaussian input process
$\mathbf{v}$	Vector of n uncorrelated standard normal random variables
$\mathbf{s}(t)$	Vector of deterministic basis functions
$h_f(\cdot)$	Impulse-response function of a filter
$h_s(\cdot)$	Impulse-response function of a system
$u(t)$	Displacement time history
$\mathbf{a}(t)$	Vector of deterministic basis functions
u_0	Threshold value
E_f	Failure event
$P(E_f)$	Failure probability
P_f^{target}	Target failure probability
$\Phi[\cdot]$	Cumulative distribution function of the standard normal distribution
β	Reliability index
β^{target}	Target reliability index
$\mathbf{d}$	Vector of deterministic design variables
$\tilde{\rho}_e(\mathbf{d})$	Element density
p	Stiffness penalization parameter
q	Mass penalization parameter
$\mathbf{D}(\cdot)$	Elastic tensor determined by material density function
$\mathbf{D}_0$	Elasticity tensor of the solid material
E_0	Young's modulus of the solid phase
$\mathbf{K}_e$	Element stiffness matrix
$\mathbf{M}_e$	Element mass matrix
$\mathbf{K}$	Global stiffness matrix
$\mathbf{M}$	Global mass matrix
$\mathbf{C}$	Global damping matrix

$\mathbf{f}$	Global load vector
$\ddot{\mathbf{u}}$	Global acceleration vector
$\dot{\mathbf{u}}$	Global velocity vector
$\mathbf{u}$	Global displacement vector
$\boldsymbol{\lambda}$	Adjoint variable vector
Φ_0	Power spectral density of the white noise process
ω_f	Predominant frequency of a random process (a filter)
ζ_f	Bandwidth of a random process (a filter)
Δ_i/L_i	Inter-story drift rations of the i-th floor evaluated at specified points
L_i	i-th floor height
Δ_i	i-th floor drift evaluated at a specified point

1 Introduction

Topology optimization aims to identify optimal material layouts of problems through mathematical programming while fulfilling given design constraints (Bendsøe and Sigmund 2003). Extensive research in the field of topology optimization has led to development of many theories, methods and algorithms to overcome well-known issues such as numerical instability in checkerboard problems (Diaz and Sigmund 1995; Jog and Haber 1996), mesh dependency problems, and ill-posed and lacking solutions in continuum settings (Kohn and Strang 1986; Sigmund and Petersson 1998). A topology problem can be well-posed by using relaxation (Bendsøe and Kikuchi 1988) or restriction of the design space (Kim and Yoon 2000; Poulsen 2002; Guest et al. 2004). An important example of such advancement in the field is the development of Solid Isotropic Material with Penalization (SIMP; Bendsøe 1989; Rozvany et al. 1992; Bendsøe and Sigmund 1999), a method designed to obtain physical properties of the intermediate densities. However, SIMP can lead to numerical instabilities such as "checker-board" effects, i.e. the formation of areas with alternating solid and void distribution in the design domain. To resolve issues associated with the checker-board (Diaz and Sigmund 1995) and the mesh-dependency, various projection schemes (Guest et al. 2004; Sigmund 2007) and filtering techniques have been developed previously (Sigmund and Petersson 1998; Bourdin 2001).

Although the field of deterministic topology optimization has been well developed, various technical challenges still exist, especially in achieving reliable solutions under uncertainty. A recent trend has shown active research efforts in finding topologies under uncertainty, which is often termed as reliability based topology optimization (RBTO) (Maute and Frangopol 2003; Allen et al. 2004; Kang et al. 2004; Kharmanda et al. 2004; Kim et al. 2006; Guest and Igusa 2008; Rozvany 2008; Lógó et al. 2009; Luo et al. 2009; Chen et al.2010; Jalalpour et al. 2013). These challenges further complicate topology optimization when it is necessary to maintain balance between architecture and engineering criteria, and to solve large-scale problems for high-rise buildings. In order to address these issues, a new method for system reliability-based topology optimization (SRBTO; Nguyen et al. 2011) was recently developed so that a probabilistic constraint on a system event consisting of multiple component events can be satisfied. This methodology provides an effective way to overcome challenges in topology optimization under probabilistic constraints on system failure events by incorporating the matrix based system reliability (MSR) method (Song and Kang 2009) into topology optimization. Despite these recent technical advances, it still remains elusive how uncertain responses of structures under random vibrations need to be addressed.

It is noted that one of the most fundamental requirements on building structures is to withstand various uncertain loads such as earthquake ground motions, wind loads and ocean waves. The structural design, therefore, needs to ensure safe and reliable operations over a prolonged period of time despite random excitations caused by hazardous events. Such a stochastic excitation is often described by a random process $f(t)$, which is the family (ensemble) of all possible random time histories (Lutes and Sarkani 2003). Alternatively, the random process can be understood as a collection of random variables defined at infinite number of points along the time axis. For instance, at a given time point $t=t_i$, $f(t_i)$ is a random variable that represents a set of possible realizations across the ensemble. Since the future realization of the random process is not completely represented by some specific cases or scenarios, predictions need to be made on the basis of probability. Therefore, a reasonable representation of the uncertainty in the random process is needed to obtain a meaningful solution for given engineering problems. This has led to active research efforts in developing random process models that can describe the uncertainty in input stochastic processes during dynamic analysis of structures subjected to random excitations.

To model and simulate stochastic processes properly, many approaches, algorithms and methods were developed previously. Some of the most widely used approaches are Monte Carlo simulation techniques (Shinozuka 1972; Kitagawa 1996; Liu and Chen 1998), autoregressive methods (Spanos and Mignolet 1987; Mignolet and Spanos 1987; Deodatis and Shinozuka 1988; Novak et al. 1995), and autoregressive moving average methods (Spanos and Mignolet 1990; Gersch and Yonemoto 1977). The spectral representation method (Shinozuka and Jan 1972; Shinozuka and Deodatis 1991 1996, 1996; Grigoriu 1993; Grigoriu 2003; Chen and Kareem 2005; Chen and Letchford 2005) has been widely utilized to simulate the random process by using a series of deterministic basis functions with uncorrelated random coefficients. The discrete representation method describes the stochastic processes in terms of a finite number of uncorrelated random variables and filters describing frequency contents and nonstationarity of the processes. Der Kiureghian (2000), Rezaeian and Der Kiureghian (2008, 2010, 2012) used the

discrete representation method along with modulating functions to model random ground motions. Konakli and Der Kiureghian (2012) used the discrete representation method to define statistical characteristic of ground motions considering various soil properties. Based on the discrete representation of input stochastic processes, Fujimura and Der Kiureghian (2007) developed a Tail-Equivalent Linearization Method (TELM) to find an equivalent linear system by matching a first-order approximation of a tail probability between a linear response and nonlinear response.

The most recent research on topology optimization has been primarily focused on structures under static loadings. Such approaches may fail to address important concerns caused by random excitations in structural design practices. For example, lateral-force-resisting structural systems should be designed to effectively control random dynamic responses caused by natural hazards or operations of non-structural components. In response to such needs and challenges, research efforts in topology optimization of structures under constraints on dynamic response have been increased recently. However, high computational cost remains as a major obstacle in incorporating dynamic/stochastic responses of structures into topology optimization. Some advances have been made in the field of research by dealing with dynamic characteristics of the structure under special loading conditions instead of actual response time histories under given deterministic or stochastic input excitations. For example, Diaz and Kikuchi (1992) dealt with eigenfrequencies as the key dynamic characteristic during topology optimization of structures under dynamic loadings. Since then, several methods and formulations related to frequencies optimization have been developed (Ma et al. 1994; Ma et al. 1995; Jensen and Pedersen 2006; Du and Olhoff 2007). Such an approach in topology optimization often aims to maximize the fundamental frequency to indirectly control dynamic responses. An alternative approach is to minimize the dynamic response of a structure for a given dominant frequency of dynamic loadings (Maeda et al. 2006; Rubio et al. 2011). Min et al. (1999) used a relaxation-homogenization theory to address minimal compliance during a given time interval in structural topology optimization problems under dynamic loadings. Such methods, however, are limited in incorporating general structural behavior addressed in actual design practices into objective functions and constraints of topology optimization.

In order to overcome these challenges, this paper introduces a new method that incorporates random vibration theories into topology optimization to satisfy probabilistic constraints defined in terms of stochastic responses. The discrete representation method of the stochastic process is adopted in the paper because the discretized form of a continuous process has practical advantages such as reducing the computational effort, facilitating implementation and identifying characteristics of the stochastic process. Moreover, an analytical sensitivity formulation is derived to enable the use of gradient-based optimizers.

The remainder of the paper is structured as follows. First, theoretical basis of the discrete representation method of random vibration is provided. It is followed by a discussion on how to characterize a linear structural system subjected to Gaussian stochastic excitations using the structural reliability theory. Next, the details of the proposed topology optimization method and a new formulation for parameter sensitivities of dynamic responses are discussed. The proposed methods are demonstrated with numerical examples and discussion of the results. Finally, the paper concludes with future directions and possible extension of our findings.

2 Discrete representation of stochastic excitations

In order to effectively incorporate stochastic processes into topology optimization, this paper adopts the discrete representation method. In particular, random ground motions are described by the discrete representation method for topology optimization of structures under seismic excitations.

2.1 Discrete representation of stochastic process

The discrete representation method describes an input stochastic process in terms of a finite number of standard normal random variables by use of a deterministic function representing the frequency content and nonstationarity (Rezaeian and Der Kiureghian 2008, 2012). This allows for evaluation of the failure probability associated with stochastic response exceeding a threshold at a given time point ("instantaneous failure probability") or crossing events during a time period ("first-passage probability") using structural reliability analysis methods, such as First- and Second-Order Reliability Methods (FORM and SORM; Der Kiureghian 2000; Der Kiureghian 2004). For example, a zero-mean stationary Gaussian input process $f(t)$ is discretized as

$$f(t) = \sum_{i=1}^{n} v_i s_i(t) = \mathbf{s}(t)^{\mathrm{T}}\mathbf{v} \tag{1}$$

where $\mathbf{v}=[v_1, v_2 \ldots, v_n]^{\mathrm{T}}$ is a vector of n uncorrelated standard normal random variables. Thus, $\mathrm{E}[v_i]=0$ and $\mathrm{E}[v_j v_k]=\delta_{jk}$ in which $\mathrm{E}[\cdot]$ denotes the mathematical expectation and δ_{jk} is the Kronecker delta. $\mathbf{s}(t)=[s_1(t),\ldots, s_n(t)]^{\mathrm{T}}$ is a vector of deterministic basis functions representing the spectral characteristics of the process. To obtain the basis function, one can use one of the available methods such as the Karhunen-Loève orthogonal expansion (Spanos and Ghanem 1989), the orthogonal series expansion approach (Zhang and Ellingwood 1994), and the optimal linear estimation method (Li and Der Kiureghian 1993).

2.2 Discrete representation of earthquake ground motions

A stochastic ground motion can be modeled as the response of a linear filter to a random pulse train. The filter may represent the characteristic of soil medium, through which the earthquake ground motion passes. For instance, the response of the linear filter excited by the white noise $W(t)$ can be expressed by a convolution integral employing the impulse-response function of the filter, $h_f(\cdot)$, i.e.

$$f(t) = \int_0^t h_f(t-\tau)W(\tau)d\tau \tag{2}$$

The power spectral density function of the white noise $W(t)$ is given as a constant, i.e. $\Phi_{WW}(\omega)=\Phi_0$. The white noise process can be represented approximately by rectangular pulses in closely spaced time steps. A random height of the pulse, which may stand for sporadic ground ruptures, is defined by the temporal average of $W(t)$ over each time interval, i.e.

$$W(t)\cong W_i = \frac{1}{\Delta t}\int_{t_i}^{t_{i+1}} W(\tau)d\tau, \quad t\in(t_i, t_{i+1}] \tag{3}$$

where $\Delta t=t_{i+1}-t_i$. Assuming $W(t)$ is a zero-mean Gaussian process, the integration of (3) results in a Gaussian random variable W_i. The mean of W_i is derived as

$$\mathrm{E}[W_i] = \mathrm{E}\left[\frac{1}{\Delta t}\int_{t_i}^{t_{i+1}} W(\tau)d\tau\right] = \frac{1}{\Delta t}\cdot\mathrm{E}\left[\int_{t_i}^{t_{i+1}} W(\tau)d\tau\right] = 0 \tag{4}$$

The variance of W_i is derived as

$$\begin{aligned}\mathrm{Var}[W_i] &= \mathrm{E}\left[\frac{1}{(\Delta t)^2}\int_{t_i}^{t_{i+1}}\int_{t_i}^{t_{i+1}} W(\tau_1)W(\tau_2)d\tau_1 d\tau_2\right]\\ &= \frac{1}{(\Delta t)^2}\int_{t_i}^{t_{i+1}}\int_{t_i}^{t_{i+1}} R_{WW}(\tau_1,\tau_2)d\tau_1 d\tau_2\\ &= \frac{1}{(\Delta t)^2}\int_{t_i}^{t_{i+1}}\int_{t_i}^{t_{i+1}} [2\pi\Phi_0\cdot\delta(\tau_2-\tau_1)]d\tau_1 d\tau_2\\ &= \frac{1}{(\Delta t)^2}\int_{t_i}^{t_{i+1}} 2\pi\Phi_0 d\tau_2 = \frac{2\pi\Phi_0}{\Delta t}\end{aligned} \tag{5}$$

where $R_{WW}(\cdot)$ is the auto-correlation function of $W(t)$, and $\delta(\cdot)$ is the Dirac delta function. In summary, W_i is the zero-mean Gaussian random variable with the variance $2\pi\Phi_0 / \Delta t$. One can also show that W_i and W_j $(i\neq j)$ are uncorrelated. Therefore, the Gaussian white noise process $W(t)$ can be represented by a set of uncorrelated standard normal random variables,

$$W_i = \sqrt{2\pi\Phi_0/\Delta t}\cdot v_i, \quad i = 1,\ldots,n \tag{6}$$

where n denotes the number of the time intervals for the time period $(0, t)$.

Substituting (3) and (6) into (2), the filter response of the Gaussian white noise process is approximately derived in a discrete form

$$\begin{aligned} f(t)&\cong\sum_{i=1}^{n} W_i\cdot h_f(t-t_i)\Delta t\\ &= \sum_{i=1}^{n}\sqrt{2\pi\Phi_0/\Delta t}\cdot v_i\cdot h_f(t-t_i)\Delta t\\ &= \sum_{i=1}^{n}\sqrt{2\pi\Phi_0\Delta t}\cdot h_f(t-t_i)\cdot v_i = \mathbf{s}(t)^{\mathrm{T}}\mathbf{v}\end{aligned} \tag{7}$$

In this case, the basis functions in the vector $\mathbf{s}(t)$ are thus derived as $s_i(t) = \sqrt{2\pi\Phi_0\Delta t}\cdot h_f(t-t_i)$.

It should be noted that the model in (7) is an example of modeling stochastic ground motions by the discrete representation method, and one can construct such a model fitted for the characteristics of ground motions at a specific site. For example, Rezaeian and Der Kiureghian (2008, 2012) incorporated non-stationarity of spatially varying ground motions into such models and developed a method for simulating an ensemble of synthetic ground motions. Konakli and Der Kiureghian (2012) developed a conditioning simulation method for generating stationary processes and extended the method to non-stationary models.

2.3 Characterization of linear system under stochastic excitations

If a stochastic excitation is described by the discrete representation method discussed above, the stochastic responses of a structural system can be also described by a finite number of random variables. For example, a displacement time history $u(t)$ of the linear system under the stochastic excitation $f(t)$ is derived as

$$\begin{aligned} u(t) &= \int_0^t f(\tau)h_s(t-\tau)d\tau = \int_0^t\left[\mathbf{s}(\tau)^{\mathrm{T}}\mathbf{v}\right]\cdot h_s(t-\tau)d\tau\\ &= \int_0^t\sum_{i=1}^{n} s_i(\tau)v_i h_s(t-\tau)d\tau = \sum_{i=1}^{n} a_i(t)\cdot v_i = \mathbf{a}(t)^{\mathrm{T}}\mathbf{v}\end{aligned} \tag{8}$$

where $h_s(t)$ is the unit impulse response function of the structural system, and $\mathbf{a}(t)$ denotes a vector of deterministic basis functions

$$a_i(t) = \int_0^t s_i(\tau)h_s(t-\tau)d\tau, \quad i = 1,\ldots,n \tag{9}$$

As a result, failure events defined in terms of dynamic response can be described in the space of standard normal random variables $\mathbf{v}$. For example, an 'instantaneous' failure event described in terms of the displacement of the linear system at time $t=t_0$, i.e. $E_f=\{u(t_0)\geq u_0\}$ where u_0 is a selected threshold can be represented by a linear half space $u_0-u(t_0)=u_0-\mathbf{a}(t_0)^{\mathrm{T}}\mathbf{v}\leq 0$, as illustrated in Fig. 1. From theories of structural reliability, the failure probability $P(E_f)$ is then obtained by a closed-form solution $P(u(t_0)\geq u_0)=\Phi[-\beta(u_0,t_0)]$ where $\Phi[\cdot]$ is the cumulative distribution function (CDF) of the standard normal distribution, and $\beta(u_0,t_0)=u_0/\|\mathbf{a}(t_0)\|$ is the reliability index. The reliability index is alternatively computed by $\beta=\hat{\boldsymbol{\alpha}}(t_0)\cdot\mathbf{v}^*$ where $\hat{\boldsymbol{\alpha}}(t_0)$ denotes the negative normalized gradient vector of the limit-state function evaluated at the so-called design point or most probable point (MPP) $\mathbf{v}^*$, which is obtained by $u_0\cdot\mathbf{a}(t_0)/\|\mathbf{a}(t_0)\|^2$ (Der Kiureghian 2000).

To facilitate finding $\mathbf{a}(t)$ in finite element settings without deriving the impulse response function necessarily, the following procedure is proposed in this paper. First, a random sample of $\mathbf{v}$ is created by generating n uncorrelated standard normal random variables. Second, an input time history $f(t)$ is computed by substituting $\mathbf{v}$ into (7). Third, the displacement time history $u(t_i)$, $i=1,2,\ldots,n$ of structures for the input time history $f(t)$ is computed using a time integration scheme such as Newmark method (1959). Then, substituting the computed time history $u(t_i)$, $i=1,2,\ldots,n$, and the random sample of $\mathbf{v}$ into (8), one can obtain

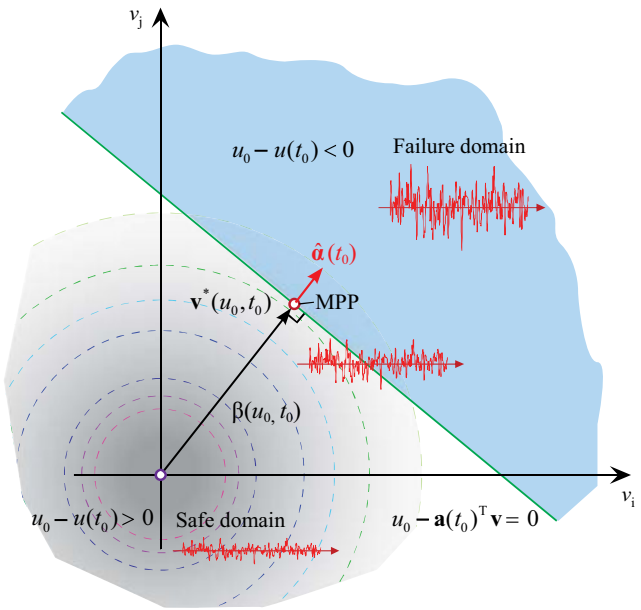

Fig. 1 Geometric representation of instantaneous failure at time t_0 (MPP: Most Probable Point)

$$
\begin{aligned}
u(t_1) &= a_1(t_1)v_1\\
u(t_2) &= a_1(t_2)v_1 + a_2(t_2)v_2\\
u(t_3) &= a_1(t_3)v_1 + a_2(t_3)v_2 + a_3(t_3)v_3\\
&\vdots\\
u(t_{n-1}) &= a_1(t_{n-1})v_1 + a_2(t_{n-1})v_2 + \ldots + a_{n-1}(t_{n-1})v_{n-1}\\
u(t_n) &= a_1(t_n)v_1 + a_2(t_n)v_2 + \ldots + a_{n-1}(t_n)v_{n-1} + a_n(t_n)v_n
\end{aligned}
\tag{10}
$$

It is noted that $a_i(t_j)=0$ for $i>j$ because $s_i(\tau)=\sqrt{2\pi\Phi_0\Delta t}\cdot h_f(\tau-t_i)$ in (9) is zero for $\tau<t_i$. When a uniform step size is used, i.e. $t_i-t_{i-1}=\Delta t$, $i=1,2,\ldots,n$ and $t_n=t_0$, it is found from (7) and (9) that

$$
a_i(j\Delta t)=a_{n+i-j}(t_0),\quad i=1,2,\ldots,n,\quad j=i,\ldots,n \tag{11}
$$

Appendix provides the details of the derivation. As a result, the system equation in (10) is given in the following matrix equation:

$$
\begin{pmatrix} u(t_1)\\ u(t_2)\\ \vdots\\ u(t_{n-1})\\ u(t_n)\end{pmatrix}
=\begin{pmatrix} u(\Delta t)\\ u(2\Delta t)\\ \vdots\\ u(t_0-\Delta t)\\ u(t_0)\end{pmatrix}
=\begin{bmatrix} a_n(t_0) & 0 & \cdots & 0 & 0\\ a_{n-1}(t_0) & a_n(t_0) & \cdots & 0 & 0\\ \vdots & \vdots & \ddots & \vdots & \vdots\\ a_2(t_0) & a_3(t_0) & \cdots & a_n(t_0) & 0\\ a_1(t_0) & a_2(t_0) & \cdots & a_{n-1}(t_0) & a_n(t_0)\end{bmatrix}
\begin{pmatrix} v_1\\ v_2\\ \vdots\\ v_{n-1}\\ v_n\end{pmatrix}
\tag{12}
$$

Each element a_i of the vector $\mathbf{a}$ can then be calculated using the forward-substitution method or solving the following equivalent matrix equations by use of a solver developed for the lower triangular matrix:

$$
\begin{pmatrix} u(t_1)\\ u(t_2)\\ \vdots\\ u(t_{n-1})\\ u(t_n)\end{pmatrix}
=\begin{pmatrix} u(\Delta t)\\ u(2\Delta t)\\ \vdots\\ u(t_0-\Delta t)\\ u(t_0)\end{pmatrix}
=\begin{bmatrix} 0 & 0 & \cdots & 0 & v_1\\ 0 & 0 & \cdots & v_1 & v_2\\ \vdots & \vdots & \ddots & \vdots & \vdots\\ 0 & v_1 & \cdots & v_{n-2} & v_{n-1}\\ v_1 & v_2 & \cdots & v_{n-1} & v_n\end{bmatrix}
\begin{pmatrix} a_1(t_0)\\ a_2(t_0)\\ \vdots\\ a_{n-1}(t_0)\\ a_n(t_0)\end{pmatrix}
\tag{13}
$$

In both methods, the absolute value of the first element in the sample, v_1 needs to be sufficiently large for numerical stability. It is found that the procedure using (13) is less sensitive to the numerical issue. The obtained vector of deterministic basis function $\mathbf{a}(t_0)$ is used in order to compute the reliability index and its associated failure probability aforementioned.

2.4 Stationarity

In general, evaluating the instantaneous failure probability $P(E_f)$ requires iterative computations through random vibration analysis and structural reliability analysis. It generates additional demands for computational resources and time in optimization. Using the discrete representation method, the instantaneous failure probability can be obtained by the closed-form solution as described in Section 2.3. It should be noted that the instantaneous failure probabilities is constant over the time period if the response achieves stationarity. This stationarity can be confirmed by investigating the autocovariance function $K_{xx}(\cdot)$ (Lutes and Sarkani 2003), which can be computed from the following form

$$K_{xx}(t_1,t_2) = \int_{-\infty}^{\infty} \Phi_{FF}(\omega) H(\omega,t_1) H(\omega,t_2) e^{i\omega(t_1-t_2)} d\omega \tag{14}$$

where $\Phi_{FF}(\omega)$ is the power spectral density function and $H(\omega,t_i), i=1,2$ denotes an incomplete Fourier transform of $h_s(t)$. Because $H(\cdot)$ is time-variant, responses of the linear system subjected to the stationary process may not be stationary in general. The stationarity of responses can be achieved when t_1, t_2 go to infinity because $H(\omega,t_1)$, $H(\omega,t_2)$ converge to a frequency response function $H(\omega)$ which does not depend on time t. For a general single degree-of-freedom oscillator, $H(\omega,t)$ can be written as

$$H(\omega,t) = H(\omega)\left[1-\left(\cos\omega_D t + \frac{\xi\omega_o + i\omega}{\omega_D}\sin\omega_D t\right) e^{-\xi\omega_o t}\cdot e^{-i\omega t}\right] \tag{15}$$

where ω_o is the natural frequency of the system, ξ denotes the damping ratio and ω_D is the damped natural frequency. Based on (15), a time t taking $e^{-\xi\omega_o t}$ to $\varepsilon \ll 1$ can be identified as the time that leads to $H(\omega,t) \cong H(\omega)$. For instance, a reduction of $e^{-\xi\omega_o t}$ to about 4% can be achieved by taking $-\xi\omega_o t = \pi$. Therefore, one can compute a sufficient time for achieving stationarity using the following expression:

$$t_{\approx 4\%} = T_o/2\xi \tag{16}$$

The primary focus of this paper is topology optimization of linear structures subjected to the stationary Gaussian process, for which the aforementioned closed-form solution of the failure probability can be used. To achieve stationarity, we compute the instantaneous failure probability at a time point after stationarity is achieved, according to (16).

3 Stochastic topology optimization framework

This section presents our proposed stochastic topology optimization framework. We incorporate the discrete representation method discussed above into topology optimization for an effective treatment of uncertainties in stochastic excitations.

3.1 Topology optimization framework

In this paper, we consider a linear elastic and isotropic constituent material with an elasticity tensor $\mathbf{D}_0$. We adopt the Solid Isotropic Material with Penalization (SIMP; Bendsøe 1989; Rozvany et al. 1992; Bendsøe and Sigmund 1999) model in which a smooth convex function is defined by a power function representation, i.e.

$$\psi(x) = x^p \tag{17}$$

where $p>0$ is a penalization factor. In order to avoid singularity of a stiffness matrix in finite element analysis, a lower bound needs to be set on the element density $\tilde{\rho}_e(\mathbf{d})$ i.e., $0 < \tilde{\rho}_{\min} \ll \tilde{\rho}_e(\mathbf{d}) < 1$ with a vector of deterministic design variables, $\mathbf{d}$. The element density can be obtained by using a density filtering method such as the projection technique (e.g. Guest et al. 2004; Sigmund 2007) to avoid checkerboard-patterns. By using a linear "hat" kernel of radius r, the element density can be computed as a weighted average of the design variables within an influence domain Ω_e such as

$$\tilde{\rho}_e(\mathbf{d}) = \frac{\sum_{j\in\Omega_e} w_j d_j}{\sum_{j\in\Omega_e} w_j} \tag{18}$$

where $w_j=(r-r_j)/r>0$ is a weight, and r_j is the distance between the centroids of element e and element j, which lies within the radius r of element e.

Therefore, an elasticity tensor of an isotropic material in the state of plane stress is determined as

$$\mathbf{D}(\tilde{\rho}_e(\mathbf{d})) = \psi(\tilde{\rho}_e(\mathbf{d}))\mathbf{D}_0 = \frac{\psi(\tilde{\rho}_e(\mathbf{d}))\cdot E_0}{1-\nu^2}\cdot\begin{bmatrix} 1 & \nu & 0 \\ \nu & 1 & 0 \\ 0 & 0 & (1-\nu)/2 \end{bmatrix} \tag{19}$$

where E_0 denotes the Young's modulus of the solid phase, ν is the Poisson's ratio, and $\mathbf{D}_0$ is the elasticity tensor of the solid material, where the density is 1. Using the SIMP model, the stiffness matrix of the e^{th} element and its sensitivity are obtained in the element-based computational framework (Bendsøe and Sigmund 2003):

$$\mathbf{K}_e(\tilde{\rho}_e) = \tilde{\rho}_e{}^{p}\,\mathbf{K}_e^0, \qquad \frac{\partial \mathbf{K}_e(\tilde{\rho}_e)}{\partial \tilde{\rho}_e} = p\tilde{\rho}_e{}^{p-1}\mathbf{K}_e^0 \tag{20}$$

where $\mathbf{K}_e^0$ is computed by

$$\mathbf{K}_e^0 = \int_{\Omega_e} \mathbf{B}^{\mathrm{T}}\mathbf{D}_0\mathbf{B}\, d\Omega_e \tag{21}$$

in which $\mathbf{B}$ denotes a strain–displacement matrix of shape function derivatives in the domain Ω_e of element e. When considering transient problems, the mass matrix and its sensitivity can be obtained as follows

$$\mathbf{M}_e(\tilde{\rho}_e) = \tilde{\rho}_e{}^{q}\mathbf{M}_e^0, \qquad \frac{\partial \mathbf{M}_e(\tilde{\rho}_e)}{\partial \tilde{\rho}_e} = q\tilde{\rho}_e{}^{q-1}\mathbf{M}_e^0 \tag{22}$$

where $\mathbf{M}_e^0$ is the mass matrix of the solid material, and q is the penalization parameter. To calculate the mass matrix in the domain of element e, a consistent mass matrix $\mathbf{M}_e^0$ is obtained as

$$\mathbf{M}_e^0 = \int_{\Omega_e} \mathbf{N}^{\mathrm{T}}\rho\mathbf{N}\, d\Omega_e \tag{23}$$

which has been adopted in this work. Here ρ is the mass density of material and $\mathbf{N}$ is the shape function of element e. The numerical examples in this paper use penalization parameter values p=3 and q=1, which are widely used in the field of topology optimization (Pedersen 2000; Du and Olhoff 2007). As usual, the global stiffness matrix $\mathbf{K}$ and mass matrix $\mathbf{M}$ for the finite element analysis can be assembled over the total number of finite elements n_e in the design domain, that is,

$$\mathbf{K} = \sum_{e=1}^{n_e}\mathbf{K}_e(\tilde{\rho}_e), \qquad \mathbf{M} = \sum_{e=1}^{n_e}\mathbf{M}_e(\tilde{\rho}_e) \tag{24}$$

3.2 Stochastic topology optimization formulation

For structures under stochastic excitations, a topology optimization problem can be formulated as

$$\begin{aligned} &\min_{\mathbf{d}} \quad f_{obj}(\tilde{\boldsymbol{\rho}}(\mathbf{d})) \\ &s.t \quad P(E_f) \le {P_f}^{\text{target}} \\ &with \quad \mathbf{M}(\tilde{\boldsymbol{\rho}})\ddot{\mathbf{u}}(t,\tilde{\boldsymbol{\rho}}) + \mathbf{C}(\tilde{\boldsymbol{\rho}})\,\dot{\mathbf{u}}\,(t,\tilde{\boldsymbol{\rho}}) + \mathbf{K}(\tilde{\boldsymbol{\rho}})\mathbf{u}(t,\tilde{\boldsymbol{\rho}}) = \mathbf{f}(t,\tilde{\boldsymbol{\rho}}) \end{aligned} \tag{25}$$

where $\tilde{\boldsymbol{\rho}}=\tilde{\boldsymbol{\rho}}(\mathbf{d})$ is the element density vector, $\mathbf{M}(\tilde{\boldsymbol{\rho}})$, $\mathbf{C}(\tilde{\boldsymbol{\rho}})$ and $\mathbf{K}(\tilde{\boldsymbol{\rho}})$ are the mass, damping and stiffness matrices of the design domain, respectively. The quantities $\ddot{\mathbf{u}}(t,\tilde{\boldsymbol{\rho}})$, $\dot{\mathbf{u}}(t,\tilde{\boldsymbol{\rho}})$, $\mathbf{u}(t,\tilde{\boldsymbol{\rho}})$ and $\mathbf{f}(t,\tilde{\boldsymbol{\rho}})$ denote the acceleration, velocity, displacement and external force vectors at time t. ${P_f}^{\text{target}}$ denotes the target failure probability which is the allowable failure probability in the probabilistic constraint. The force vector for the structure subjected to ground acceleration $\ddot{u}_g(t)$ generated in the form of (7) can be expressed as $\mathbf{f}(t,\tilde{\boldsymbol{\rho}}) = -\mathbf{M}(\tilde{\boldsymbol{\rho}})\mathbf{l}\ddot{u}_g(t)$, in which the vector $\mathbf{l}$ represents the directional distribution of masses with unity. It can be derived from the behavior of structures subjected to earthquake excitation of the base of the structure. The total displacement of the mass $\mathbf{M}$ by $\mathbf{u}^t(t,\tilde{\boldsymbol{\rho}})$ is a summation of the relative displacement between the ground and the mass by $\mathbf{u}(t,\tilde{\boldsymbol{\rho}})$ and the displacement of the ground denoted by $u_g(t)\mathbf{l}$. Because elastic and damping forces are only generated by the relative motion $\mathbf{u}(t,\tilde{\boldsymbol{\rho}})$, the inertial force related to the acceleration becomes $\mathbf{M}(\tilde{\boldsymbol{\rho}})\big(\ddot{\mathbf{u}}(t) + \mathbf{l}\ddot{u}_g(t)\big)$. Thus, the external force vector is expressed as $\mathbf{f}(t,\tilde{\boldsymbol{\rho}}) = -\mathbf{M}(\tilde{\boldsymbol{\rho}})\mathbf{l}\ddot{u}_g(t)$. In this paper, the damping matrix is constructed by using a Rayleigh damping model, $\mathbf{C}=\kappa_0\mathbf{M}+\kappa_1\mathbf{K}$. The coefficients κ_0 and κ_1 in the Rayleigh damping model are determined under the assumption of 2 % damping ratio for structures.

Optimization of nonlinear systems and/or systems subjected to non-stationary or non-Gaussian processes can also be achieved by modulating various filters (Rezaeian and Der Kiureghian 2008, 2010) and utilizing structural reliability analysis methods such as FORM and SORM. In order to update design variables during optimization procedures, nonlinear optimization algorithms such as the sequential quadratic programming (SQP) or the method of moving asymptotes (MMA; Svanberg 1987) can be used. In this paper, MMA is used along with the special purpose sensitivity formulation described below. The MMA was chosen because the algorithm can handle the multiple constraints effectively and shows faster convergence compared to the SQP and the interior point method in the numerical examples.

3.3 Overall topology optimization process

Figure 2 illustrates the proposed procedure of topology optimization of structures under stochastic excitations. The procedure begins with an initial design and a stochastic model of excitation. For instance, the Kanai-Tajimi power spectral density model (Clough and Penzien 1993) can be implemented to approximately match the spectral characteristics of ground motions. The failure probability, i.e. the probability that the current design violates the given probabilistic constraint, is computed by structural reliability analysis (Der Kiureghian 2000; Der Kiureghian 2004). As described above, the instantaneous failure probability of the linear structure under the Gaussian excitations can be computed by the closed-form solution. Next, the objective function, constraint functions and their sensitivities are computed to update design variables using an optimization algorithm such as MMA. The convergence check based on the total change in the material

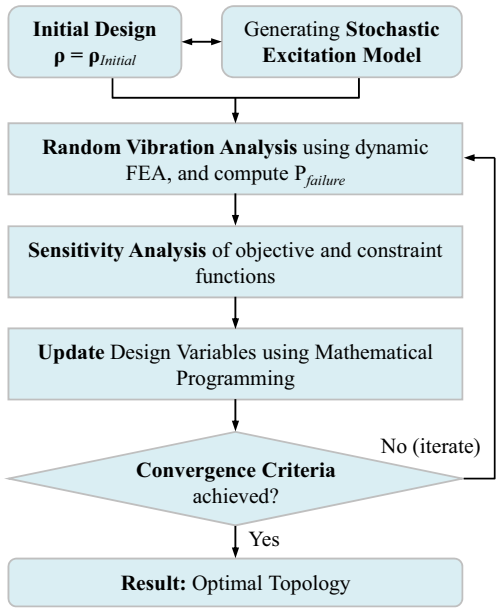

Fig. 2 Flow chart for topology optimization under stochastic excitations

distribution is performed at the end of each iteration step. This process is repeated until a tolerance threshold of 0.5 % is reached.

4 Sensitivity calculations

Computing the sensitivity of structural responses with respect to various design parameters is essential for efficient gradient-based optimization. Therefore, various approaches have been developed for computing sensitivity of static as well as dynamic responses (Haug and Arora 1978; Haftka and Gürdal 1992). Computing gradients of responses of the system under stochastic process, however, differs from aforementioned sensitivity calculations, in that this system requires an additional layer of complexity due to the randomness of the input process. In this paper, a new sensitivity formulation employing the adjoint method is developed for linear structures subjected to stochastic excitations modeled by the discrete representation method.

Consider the following constraint on the probability of the instantaneous failure event described by the discrete representation method:

$$P(E_f) = P(u_0 - \mathbf{a}(t_0, \tilde{\boldsymbol{\rho}})^{\mathrm{T}}\mathbf{v} \le 0) \le P_f{}^{\mathrm{target}} \tag{26}$$

Alternatively, the constraint in (26) can also be described using the CDF of the standard normal distribution and the reliability index, i.e.

$$\Phi\left[-\beta(u_0, t_0, \tilde{\boldsymbol{\rho}})\right] \le \Phi\left[-\beta^{\mathrm{target}}\right] \quad \text{or} \quad \beta(u_0, t_0, \tilde{\boldsymbol{\rho}}) \ge \beta^{\mathrm{target}} \tag{27}$$

where β^{target} denotes the target reliability index, which is $(1-P_f^{\mathrm{target}})$ quantile of the standard normal distribution, i.e.. $\Phi[-\beta^{\mathrm{target}}]=P_f^{\mathrm{target}}$. Therefore, the sensitivity of the reliability index with respect to the design variables **d** needs to be evaluated to enable the use of gradient-based optimization algorithms. As described above, the reliability index is computed as

$$\begin{aligned}\beta(u_0, t_0, \tilde{\boldsymbol{\rho}}) &= \frac{u_0}{\left\|\mathbf{a}(t_0, \tilde{\boldsymbol{\rho}})\right\|} \\ &= \frac{u_0}{\sqrt{a_1(t_0, \tilde{\boldsymbol{\rho}})^2 + a_2(t_0, \tilde{\boldsymbol{\rho}})^2 + \cdots + a_n(t_0, \tilde{\boldsymbol{\rho}})^2}}\end{aligned} \tag{28}$$

By applying the chain rule to (28), the sensitivity of the reliability index with respect to the design variable $d_e \in \mathbf{d}$ is derived as

$$\begin{aligned}\frac{\partial\beta(u_0, t_0, \tilde{\boldsymbol{\rho}})}{\partial d_e} &= \sum_{k=1}^{n_e} \frac{\partial\beta(u_0, t_0, \tilde{\boldsymbol{\rho}})}{\partial\tilde{\rho}_k} \cdot \frac{\partial\tilde{\rho}_k}{\partial d_e} \\ &= \left[-\frac{u_0}{(a_1(t_0, \tilde{\boldsymbol{\rho}})^2 + \cdots + a_n(t_0, \tilde{\boldsymbol{\rho}})^2)^{3/2}}\right] \cdot \sum_{k=1}^{n_e}\sum_{i=1}^{n} \left(a_i(t_0, \tilde{\boldsymbol{\rho}}) \cdot \frac{\partial a_i(t_0, \tilde{\boldsymbol{\rho}})}{\partial\tilde{\rho}_k}\right) \cdot \frac{\partial\tilde{\rho}_k}{\partial d_e} \\ &= \sum_{k=1}^{n_e}\sum_{i=1}^{n} \left(c_i(u_0, t_0, \tilde{\boldsymbol{\rho}}) \cdot \frac{\partial a_i(t_0, \tilde{\boldsymbol{\rho}})}{\partial\tilde{\rho}_k}\right) \cdot \frac{\partial\tilde{\rho}_k}{\partial d_e}\end{aligned} \tag{29}$$

where

$$c_i(u_0, t_0, \tilde{\boldsymbol{\rho}}) = -u_0 \cdot a_i(t_0, \tilde{\boldsymbol{\rho}}) \left[a_1(t_0, \tilde{\boldsymbol{\rho}})^2 + \cdots + a_n(t_0, \tilde{\boldsymbol{\rho}})^2\right]^{-3/2} \tag{30}$$

In (29), the index k represents the k-th element, $k=1,\ldots,n_e$, and the partial derivative $\partial\tilde{\rho}_k/\partial d_e$ can be obtained from the filtering function in (18).

However, the sensitivity formulation in (29) cannot be completed as is because of the implicitly defined sensitivities with respect to the element density, i.e. $\partial a_i(t_0, \tilde{\boldsymbol{\rho}})/\partial\tilde{\rho}_k$. To enable the sensitivity calculation, a new sensitivity calculation procedure based on the adjoint method is developed as presented below.

4.1 Adjoint sensitivity analysis

The basic idea of the adjoint method is introducing an adjoint system of equations so that computing implicitly defined terms in the sensitivity analysis can be avoided and thus computational cost can be reduced (Haug et al. 1986; Haftka and Gürdal 1992; Choi and Kim 2005). In the sensitivity analysis of the reliability index, the discretized system in the last line of (25) is considered as the adjoint system. The equation of motion can be

solved numerically using one of the time integration schemes such as the central difference method (Hulbert and Chung 1996), Houbolt method (Houbolt 1950) or Newmark method (Newmark 1959). The implicit Newmark time integration method is presented here because the approach shows more stable and accurate results for the numerical examples. The Newmark method is based on the following time-stepping rules:

$$\dot{\mathbf{u}}\,(t_{j+1}) = \dot{\mathbf{u}}\,(t_j) + [(1-\gamma)\Delta t]\ddot{\mathbf{u}}(t_j) + (\gamma\Delta t)\ddot{\mathbf{u}}(t_{j+1}) \tag{31}$$

$$\mathbf{u}(t_{j+1}) = \mathbf{u}(t_j) + \Delta t\,\dot{\mathbf{u}}\,(t_j) + \left[(0.5-\eta)\Delta t^2\right]\ddot{\mathbf{u}}(t_j) + \left[\eta\Delta t^2\right]\ddot{\mathbf{u}}(t_{j+1}) \tag{32}$$

The parameters γ and η determine the stability and accuracy characteristic of the method (γ=0.5 and η=0.25 are used in the research). Substituting (31)-(32) for $\ddot{\mathbf{u}}(t_{j+1})$ and $\dot{\mathbf{u}}(t_{j+1})$ into the second-order governing equation in (25) at $t=t_{j+1}$, one can obtain the following expression

$$\begin{aligned}\left(\frac{1}{\eta(\Delta t)^2}\mathbf{M}(\tilde{\boldsymbol{\rho}}) + \frac{\gamma}{\eta\Delta t}\mathbf{C}(\tilde{\boldsymbol{\rho}}) + \mathbf{K}(\tilde{\boldsymbol{\rho}})\right)\mathbf{u}(t_{j+1},\tilde{\boldsymbol{\rho}}) &= \mathbf{f}(t_{j+1},\tilde{\boldsymbol{\rho}}) \\ &+ \mathbf{C}(\tilde{\boldsymbol{\rho}})\left[\frac{\gamma}{\eta\Delta t}\mathbf{u}(t_j,\tilde{\boldsymbol{\rho}}) + \left(\frac{\gamma}{\eta}-1\right)\dot{\mathbf{u}}\,(t_j,\tilde{\boldsymbol{\rho}}) + \Delta t\left(\frac{\gamma}{2\eta}-1\right)\ddot{\mathbf{u}}(t_j,\tilde{\boldsymbol{\rho}})\right] \\ &+ \mathbf{M}(\tilde{\boldsymbol{\rho}})\left[\frac{1}{\eta(\Delta t)^2}\mathbf{u}(t_j,\tilde{\boldsymbol{\rho}}) + \frac{1}{\eta\Delta t}\dot{\mathbf{u}}\,(t_j,\tilde{\boldsymbol{\rho}}) + \left(\frac{1}{2\eta}-1\right)\ddot{\mathbf{u}}(t_j,\tilde{\boldsymbol{\rho}})\right]\end{aligned} \tag{33}$$

Based on a general recurrence relation associated with three sequential displacements (Chan et al. 1962; Zienkiewicz 1977), the equilibrium equations of motion can be solved for $\mathbf{u}(t_{j+1},\tilde{\boldsymbol{\rho}})$:

$$\begin{aligned}\left(\mathbf{M}(\tilde{\boldsymbol{\rho}}) + \gamma\Delta t\mathbf{C}(\tilde{\boldsymbol{\rho}}) + \eta(\Delta t)^2\mathbf{K}(\tilde{\boldsymbol{\rho}})\right)\mathbf{u}(t_{j+1},\tilde{\boldsymbol{\rho}}) &= \eta(\Delta t)^2\mathbf{f}(t_{j+1},\tilde{\boldsymbol{\rho}}) \\ &+ (0.5+\gamma-2\eta)(\Delta t)^2\mathbf{f}(t_j,\tilde{\boldsymbol{\rho}}) + (0.5-\gamma+\eta)(\Delta t)^2\mathbf{f}(t_{j-1},\tilde{\boldsymbol{\rho}}) \\ &-\left[-2\mathbf{M}(\tilde{\boldsymbol{\rho}}) + (1-2\gamma)\Delta t\mathbf{C}(\tilde{\boldsymbol{\rho}}) + (0.5+\gamma-2\eta)(\Delta t)^2\mathbf{K}(\tilde{\boldsymbol{\rho}})\right]\mathbf{u}(t_j,\tilde{\boldsymbol{\rho}}) \\ &-\left[\mathbf{M}(\tilde{\boldsymbol{\rho}}) + (\gamma-1)\Delta t\mathbf{C}(\tilde{\boldsymbol{\rho}}) + (0.5-\gamma+\eta)(\Delta t)^2\mathbf{K}(\tilde{\boldsymbol{\rho}})\right]\mathbf{u}(t_{j-1},\tilde{\boldsymbol{\rho}})\end{aligned} \tag{34}$$

It should be noted that the force vector $\mathbf{f}(t_{j+1},\tilde{\boldsymbol{\rho}})$ can be replaced by the inertia force vector $-\mathbf{M}(\tilde{\boldsymbol{\rho}})\mathbf{1}f(t_{j+1})$ for structures subjected to ground excitations aforementioned. The following notations are introduced in order to simplify the derivations:

$$\begin{aligned}\underline{\underline{\mathbf{A}}}(\tilde{\boldsymbol{\rho}}) &= \mathbf{M}(\tilde{\boldsymbol{\rho}}) + \gamma\Delta t\cdot\mathbf{C}(\tilde{\boldsymbol{\rho}}) + \eta(\Delta t)^2\mathbf{K}(\tilde{\boldsymbol{\rho}}) \\ \underline{\underline{\mathbf{B}}}(\tilde{\boldsymbol{\rho}}) &= -2\mathbf{M}(\tilde{\boldsymbol{\rho}}) + (1-2\gamma)\Delta t\mathbf{C}(\tilde{\boldsymbol{\rho}}) + (0.5+\gamma-2\eta)(\Delta t)^2\mathbf{K}(\tilde{\boldsymbol{\rho}}) \\ \underline{\underline{\mathbf{E}}}(\tilde{\boldsymbol{\rho}}) &= \mathbf{M}(\tilde{\boldsymbol{\rho}}) + (\gamma-1)\Delta t\mathbf{C}(\tilde{\boldsymbol{\rho}}) + (0.5-\gamma+\eta)(\Delta t)^2\mathbf{K}(\tilde{\boldsymbol{\rho}})\end{aligned} \tag{35}$$

Substituting (34) with (35) and differentiating the equation with respect to the element density, one can obtain the discretized adjoint system as follows:

$$\begin{aligned}&\frac{\partial\underline{\underline{\mathbf{A}}}(\tilde{\boldsymbol{\rho}})}{\partial\tilde{\rho}_k}\cdot\mathbf{u}(t_{j+1},\tilde{\boldsymbol{\rho}}) + \underline{\underline{\mathbf{A}}}(\tilde{\boldsymbol{\rho}})\cdot\frac{\partial\mathbf{u}(t_{j+1},\tilde{\boldsymbol{\rho}})}{\partial\tilde{\rho}_k} - \eta(\Delta t)^2\frac{\partial\mathbf{f}(t_{j+1},\tilde{\boldsymbol{\rho}})}{\partial\tilde{\rho}_k} \\ &-(0.5+\gamma-2\eta)(\Delta t)^2\frac{\partial\mathbf{f}(t_j,\tilde{\boldsymbol{\rho}})}{\partial\tilde{\rho}_k} - (0.5-\gamma+\eta)(\Delta t)^2\frac{\partial\mathbf{f}(t_{j-1},\tilde{\boldsymbol{\rho}})}{\partial\tilde{\rho}_k} + \frac{\partial\underline{\underline{\mathbf{B}}}(\tilde{\boldsymbol{\rho}})}{\partial\tilde{\rho}_k}\cdot\mathbf{u}(t_j,\tilde{\boldsymbol{\rho}}) \\ &+\underline{\underline{\mathbf{B}}}(\tilde{\boldsymbol{\rho}})\cdot\frac{\partial\mathbf{u}(t_j,\tilde{\boldsymbol{\rho}})}{\partial\tilde{\rho}_k} + \frac{\partial\underline{\underline{\mathbf{E}}}(\tilde{\boldsymbol{\rho}})}{\partial\tilde{\rho}_k}\cdot\mathbf{u}(t_{j-1},\tilde{\boldsymbol{\rho}}) + \underline{\underline{\mathbf{E}}}(\tilde{\boldsymbol{\rho}})\cdot\frac{\partial\mathbf{u}(t_{j-1},\tilde{\boldsymbol{\rho}})}{\partial\tilde{\rho}_k} = 0\end{aligned} \tag{36}$$

It should be noted that this adjoit system is self-adjoint because **M**, **C** and **K** are symmetric based on (21) and (23). Premultiplying the discretized adjoint system with a n_{dof} dimensional adjoint variable vector $\boldsymbol{\lambda}_{n-j+1}$ and adding to right-hand side terms of (29), one obtains

$$\begin{aligned}\frac{\partial\beta(u_0,t_0,\tilde{\boldsymbol{\rho}})}{\partial\tilde{\rho}_k} &= \sum_{i=1}^{n}\left(c_i(u_0,t_0,\tilde{\boldsymbol{\rho}})\cdot\frac{\partial a_i(t_0,\tilde{\boldsymbol{\rho}})}{\partial\tilde{\rho}_k}\right) \\ &+ \sum_{j=1}^{n}\boldsymbol{\lambda}_{n-j+1}^{\mathrm{T}}\left[\frac{\partial\underline{\underline{\mathbf{A}}}(\tilde{\boldsymbol{\rho}})}{\partial\tilde{\rho}_k}\cdot\mathbf{u}(t_j,\tilde{\boldsymbol{\rho}}) + \underline{\underline{\mathbf{A}}}(\tilde{\boldsymbol{\rho}})\cdot\frac{\partial\mathbf{u}(t_j,\tilde{\boldsymbol{\rho}})}{\partial\tilde{\rho}_k}\right. \\ &-\eta(\Delta t)^2\frac{\partial\mathbf{f}(t_j,\tilde{\boldsymbol{\rho}})}{\partial\tilde{\rho}_k} - (0.5+\gamma-2\eta)(\Delta t)^2\frac{\partial\mathbf{f}(t_{j-1},\tilde{\boldsymbol{\rho}})}{\partial\tilde{\rho}_k} \\ &-(0.5-\gamma+\eta)(\Delta t)^2\frac{\partial\mathbf{f}(t_{j-2},\tilde{\boldsymbol{\rho}})}{\partial\tilde{\rho}_k} + \frac{\partial\underline{\underline{\mathbf{B}}}(\tilde{\boldsymbol{\rho}})}{\partial\tilde{\rho}_k}\cdot\mathbf{u}(t_{j-1},\tilde{\boldsymbol{\rho}}) \\ &\left.+\underline{\underline{\mathbf{B}}}(\tilde{\boldsymbol{\rho}})\cdot\frac{\partial\mathbf{u}(t_{j-1},\tilde{\boldsymbol{\rho}})}{\partial\tilde{\rho}_k} + \frac{\partial\underline{\underline{\mathbf{E}}}(\tilde{\boldsymbol{\rho}})}{\partial\tilde{\rho}_k}\cdot\mathbf{u}(t_{j-2},\tilde{\boldsymbol{\rho}}) + \underline{\underline{\mathbf{E}}}(\tilde{\boldsymbol{\rho}})\cdot\frac{\partial\mathbf{u}(t_{j-2},\tilde{\boldsymbol{\rho}})}{\partial\tilde{\rho}_k}\right]\end{aligned} \tag{37}$$

It is noted that the first summation on the right-hand side of (37) includes gradients of $\mathbf{a}(t)$ which was introduced to describe a certain degree-of-freedom, i.e. $u(t)=\mathbf{a}(t)^{\mathrm{T}}\mathbf{v}$ while the added terms in the second summation are expressed with gradients of displacement vector **u** including all degrees-of-freedom. To derive the sensitivity in (37) in terms of derivatives of $\mathbf{u}(t)$, the terms in the first summation are alternatively described as

$$\sum_{i=1}^{n}\left(c_i(t_0,\tilde{\boldsymbol{\rho}})\cdot\frac{\partial a_i(t_0,\tilde{\boldsymbol{\rho}})}{\partial\tilde{\rho}_k}\right) = \sum_{i=1}^{n}\left(T_i\cdot\mathbf{z}^{\mathrm{T}}\cdot\frac{\partial\mathbf{u}(t_i,\tilde{\boldsymbol{\rho}})}{\partial\tilde{\rho}_k}\right) \tag{38}$$

where **z** is a binary vector that indicates which degree-of-freedom (DOF) that $\mathbf{a}(t)$ indicates. If the sensitivity of the k-th degree-of-freedom is of interest, all elements of **z** vector are zeroes except the k-th element, which is 1. From (8), the sensitivity of a selected degree-of-freedom of the displacement vector, i.e. $u(t)\in\mathbf{u}(t)$, is determined as

$$\frac{\partial u(t,\tilde{\boldsymbol{\rho}})}{\partial\tilde{\rho}_k} = \frac{\partial\mathbf{a}(t,\tilde{\boldsymbol{\rho}})^{\mathrm{T}}}{\partial\tilde{\rho}_k}\mathbf{v} \tag{39}$$

By means of a procedure similar to the one described in (10)-(13), the following matrix equation is derived to obtain $\partial a_i(t_0, \tilde{\boldsymbol{\rho}})/\partial\tilde{\rho}_k$, $i=1\ldots,n$:

$$\begin{pmatrix} \partial u(t_1)/\partial\tilde{\rho}_k \\ \partial u(t_2)/\partial\tilde{\rho}_k \\ \vdots \\ \partial u(t_{n-1})/\partial\tilde{\rho}_k \\ \partial u(t_n)/\partial\tilde{\rho}_k \end{pmatrix} = \begin{bmatrix} \partial a_n(t_0)/\partial\tilde{\rho}_k & 0 & \cdots & 0 & 0 \\ \partial a_{n-1}(t_0)/\partial\tilde{\rho}_k & \partial a_n(t_0)/\partial\tilde{\rho}_k & \cdots & 0 & 0 \\ \vdots & \vdots & \ddots & \vdots & \vdots \\ \partial a_2(t_0)/\partial\tilde{\rho}_k & \partial a_3(t_0)/\partial\tilde{\rho}_k & \cdots & \partial a_n(t_0)/\partial\tilde{\rho}_k & 0 \\ \partial a_1(t_0)/\partial\tilde{\rho}_k & \partial a_2(t_0)/\partial\tilde{\rho}_k & \cdots & \partial a_{n-1}(t_0)/\partial\tilde{\rho}_k & \partial a_n(t_0)/\partial\tilde{\rho}_k \end{bmatrix} \begin{pmatrix} v_1 \\ v_2 \\ \vdots \\ v_{n-1} \\ v_n \end{pmatrix} \tag{40}$$

Substituting (40) into (38), one obtains the following expression

$$\begin{aligned} &c_1(t_0, \tilde{\boldsymbol{\rho}})\cdot\frac{\partial a_1(t_0, \tilde{\boldsymbol{\rho}})}{\partial\tilde{\rho}_k} + c_2(t_0, \tilde{\boldsymbol{\rho}})\cdot\frac{\partial a_2(t_0, \tilde{\boldsymbol{\rho}})}{\partial\tilde{\rho}_k} + \ldots + c_n(t_0, \tilde{\boldsymbol{\rho}})\cdot\frac{\partial a_n(t_0, \tilde{\boldsymbol{\rho}})}{\partial\tilde{\rho}_k} = \\ &T_1\cdot\frac{\partial a_n(t_0, \tilde{\boldsymbol{\rho}})}{\partial\tilde{\rho}_k}\cdot v_1 + T_2\cdot\left(\frac{\partial a_{n-1}(t_0, \tilde{\boldsymbol{\rho}})}{\partial\tilde{\rho}_k}\cdot v_1 + \frac{\partial a_n(t_0, \tilde{\boldsymbol{\rho}})}{\partial\tilde{\rho}_k}\cdot v_2\right) + \ldots + \\ &T_n\cdot\left(\frac{\partial a_1(t_0, \tilde{\boldsymbol{\rho}})}{\partial\tilde{\rho}_k}\cdot v_1 + \frac{\partial a_2(t_0, \tilde{\boldsymbol{\rho}})}{\partial\tilde{\rho}_k}\cdot v_2 + \ldots \frac{\partial a_n(t_0, \tilde{\boldsymbol{\rho}})}{\partial\tilde{\rho}_k}\cdot v_n\right) \end{aligned} \tag{41}$$

Comparing the coefficients of the left and right hand sides of (41), one can find

$$\begin{aligned} &T_n v_1 = c_1(t_0, \tilde{\boldsymbol{\rho}}) \\ &T_{n-1}v_1 + T_n v_2 = c_2(t_0, \tilde{\boldsymbol{\rho}}) \\ &\vdots \\ &T_1 v_1 + T_2 v_2 + \ldots + T_n v_n = c_n(t_0, \tilde{\boldsymbol{\rho}}) \end{aligned} \tag{42}$$

The coefficients T_i, $i=1,\ldots,n$, can be obtained by solving (42). Substituting (38) into (37) and isolating implicitly defined terms $\partial\mathbf{u}(t_j, \tilde{\boldsymbol{\rho}})/\partial\tilde{\rho}_k$, one obtains:

$$\begin{aligned} \frac{\partial\beta(u_0, t_0, \tilde{\boldsymbol{\rho}})}{\partial\tilde{\rho}_k} &= \sum_{i=1}^{n}\left(T_i\cdot\mathbf{z}^{\mathrm{T}}\frac{\partial\mathbf{u}(t_i, \tilde{\boldsymbol{\rho}})}{\partial\tilde{\rho}_k}\right) \\ &+ \sum_{j=1}^{n}\boldsymbol{\lambda}_{n-j+1}^{\mathrm{T}}\left[\frac{\partial\underline{\underline{\mathbf{A}}}(\tilde{\boldsymbol{\rho}})}{\partial\tilde{\rho}_k}\cdot\mathbf{u}(t_j, \tilde{\boldsymbol{\rho}}) - \eta(\Delta t)^2\frac{\partial\mathbf{f}(t_j, \tilde{\boldsymbol{\rho}})}{\partial\tilde{\rho}_k}\right. \\ &-(0.5+\gamma-2\eta)(\Delta t)^2\frac{\partial\mathbf{f}(t_{j-1}, \tilde{\boldsymbol{\rho}})}{\partial\tilde{\rho}_k} \\ &\left.-(0.5-\gamma+\eta)(\Delta t)^2\frac{\partial\mathbf{f}(t_{j-2}, \tilde{\boldsymbol{\rho}})}{\partial\tilde{\rho}_k} + \frac{\partial\underline{\underline{\mathbf{B}}}(\tilde{\boldsymbol{\rho}})}{\partial\tilde{\rho}_k}\cdot\mathbf{u}(t_{j-1}, \tilde{\boldsymbol{\rho}}) + \frac{\partial\underline{\underline{\mathbf{E}}}(\tilde{\boldsymbol{\rho}})}{\partial\tilde{\rho}_k}\cdot\mathbf{u}(t_{j-2}, \tilde{\boldsymbol{\rho}})\right] \\ &+ \sum_{j=1}^{n}\boldsymbol{\lambda}_{n-j+1}^{\mathrm{T}}\left[\underline{\underline{\mathbf{A}}}(\tilde{\boldsymbol{\rho}})\cdot\frac{\partial\mathbf{u}(t_j, \tilde{\boldsymbol{\rho}})}{\partial\tilde{\rho}_k} + \underline{\underline{\mathbf{B}}}(\tilde{\boldsymbol{\rho}})\cdot\frac{\partial\mathbf{u}(t_{j-1}, \tilde{\boldsymbol{\rho}})}{\partial\tilde{\rho}_k} + \underline{\underline{\mathbf{E}}}(\tilde{\boldsymbol{\rho}})\cdot\frac{\partial\mathbf{u}(t_{j-2}, \tilde{\boldsymbol{\rho}})}{\partial\tilde{\rho}_k}\right] \end{aligned} \tag{43}$$

It is noted that this procedure requires knowledge of $\mathbf{u}(t_{-1}, \tilde{\boldsymbol{\rho}})$, $\mathbf{u}(0, \tilde{\boldsymbol{\rho}})$ and their partial derivatives so that a special starting procedure such as initial displacements by the central difference method can be used to generate initial results. The terms including $\partial\mathbf{u}(t_j, \tilde{\boldsymbol{\rho}})/\partial\tilde{\rho}_k, j=1,\ldots,n$, are identified and grouped in (43). Then, the value of the adjoint vector $\boldsymbol{\lambda}_n$ is found, such that the coefficients of unknown derivatives $\partial\mathbf{u}(t_j, \tilde{\boldsymbol{\rho}})/\partial\tilde{\rho}_k$, $j=1,\ldots,n$, are zero, i.e.

$$\begin{aligned} &T_n\cdot\mathbf{z}^{\mathrm{T}} + \boldsymbol{\lambda}_1^{\mathrm{T}}\cdot\underline{\underline{\mathbf{A}}}(\tilde{\boldsymbol{\rho}}) = 0 \\ &T_{n-1}\cdot\mathbf{z}^{\mathrm{T}} + \boldsymbol{\lambda}_2^{\mathrm{T}}\cdot\underline{\underline{\mathbf{A}}}(\tilde{\boldsymbol{\rho}}) + \boldsymbol{\lambda}_1^{\mathrm{T}}\cdot\underline{\underline{\mathbf{B}}}(\tilde{\boldsymbol{\rho}}) = 0 \\ &T_{n-2}\cdot\mathbf{z}^{\mathrm{T}} + \boldsymbol{\lambda}_3^{\mathrm{T}}\cdot\underline{\underline{\mathbf{A}}}(\tilde{\boldsymbol{\rho}}) + \boldsymbol{\lambda}_2^{\mathrm{T}}\cdot\underline{\underline{\mathbf{B}}}(\tilde{\boldsymbol{\rho}}) + \boldsymbol{\lambda}_1^{\mathrm{T}}\cdot\underline{\underline{\mathbf{E}}}(\tilde{\boldsymbol{\rho}}) = 0 \\ &\vdots \\ &T_1\cdot\mathbf{z}^{\mathrm{T}} + \boldsymbol{\lambda}_n^{\mathrm{T}}\cdot\underline{\underline{\mathbf{A}}}(\tilde{\boldsymbol{\rho}}) + \boldsymbol{\lambda}_{n-1}^{\mathrm{T}}\cdot\underline{\underline{\mathbf{B}}}(\tilde{\boldsymbol{\rho}}) + \boldsymbol{\lambda}_{n-2}^{\mathrm{T}}\cdot\underline{\underline{\mathbf{E}}}(\tilde{\boldsymbol{\rho}}) = 0 \end{aligned} \tag{44}$$

Finally, substituting the value of the adjoint vector obtained from (44) into (43) gives the sensitivity from the following equation that does not involve implicitly defined derivative terms:

$$\begin{aligned} \frac{\partial\beta(u_0, t_0, \tilde{\boldsymbol{\rho}})}{\partial\tilde{\rho}_k} &= \sum_{j=1}^{n}\boldsymbol{\lambda}_{n-j+1}{}^{\mathrm{T}}\left[\frac{\partial\underline{\underline{\mathbf{A}}}(\tilde{\boldsymbol{\rho}})}{\partial\tilde{\rho}_k}\cdot\mathbf{u}(t_j, \tilde{\boldsymbol{\rho}}) - \eta(\Delta t)^2\frac{\partial\mathbf{f}(t_j, \tilde{\boldsymbol{\rho}})}{\partial\tilde{\rho}_k}\right. \\ &-(0.5+\gamma-2\eta)(\Delta t)^2\frac{\partial\mathbf{f}(t_{j-1}, \tilde{\boldsymbol{\rho}})}{\partial\tilde{\rho}_k} \\ &\left.-(0.5-\gamma+\eta)(\Delta t)^2\frac{\partial\mathbf{f}(t_{j-2}, \tilde{\boldsymbol{\rho}})}{\partial\tilde{\rho}_k} + \frac{\partial\underline{\underline{\mathbf{B}}}(\tilde{\boldsymbol{\rho}})}{\partial\tilde{\rho}_k}\cdot\mathbf{u}(t_{j-1}, \tilde{\boldsymbol{\rho}}) + \frac{\partial\underline{\underline{\mathbf{E}}}(\tilde{\boldsymbol{\rho}})}{\partial\tilde{\rho}_k}\cdot\mathbf{u}(t_{j-2}, \tilde{\boldsymbol{\rho}})\right] \\ &+ \boldsymbol{\lambda}_n{}^{\mathrm{T}}\left[\underline{\underline{\mathbf{B}}}(\tilde{\boldsymbol{\rho}})\cdot\frac{\partial\mathbf{u}(0, \tilde{\boldsymbol{\rho}})}{\partial\tilde{\rho}_k} + \underline{\underline{\mathbf{E}}}(\tilde{\boldsymbol{\rho}})\cdot\frac{\partial\mathbf{u}(t_{j-1}, \tilde{\boldsymbol{\rho}})}{\partial\tilde{\rho}_k}\right] + \boldsymbol{\lambda}_{n-1}{}^{\mathrm{T}}\left[\underline{\underline{\mathbf{E}}}(\tilde{\boldsymbol{\rho}})\cdot\frac{\partial\mathbf{u}(0, \tilde{\boldsymbol{\rho}})}{\partial\tilde{\rho}_k}\right] \end{aligned} \tag{45}$$

4.2 Performance of the proposed method for sensitivity calculations

The performance of the proposed method for the sensitivity calculation is tested with a numerical example in terms of efficiency and accuracy. For this purpose, the example considers a structure shown in Fig. 3 (a), which is subjected to the filtered stationary process which is represented in the form of (1) with the basis functions $s_i(t)=\exp[-2.4\pi(t-t_i)]\cdot\sin[3.2\pi(t-t_i)]\cdot H(t-t_i)$ (Der Kiureghian 2000) where $H(\cdot)$ is a unit step function. The basis functions are normalized such that $\|\mathbf{s}(t)\|=1$. The continuum structure is discretized with quadrilateral elements (Q4). The frame elements illustrated as straight lines in Fig. 3(a) are divided into smaller elements. Those are then connected to the nodes of Q4 elements along the straight lines. The thickness of the Q4 element is 0.1 m, the size of frame elements is 0.45 m × 0.45 m, and Young's modulus $E=21{,}000$ MPa and density $\rho=2{,}400$ kg/m^3 are used to describe the material properties of the structure. The uniform distribution of the material density 0.5 over the Q4 domain is assumed in the sensitivity calculation. The probabilistic constraint is given on tip-displacements, which are evaluated at red dots as shown in Fig. 3(a). The failure event E_f occurs when the

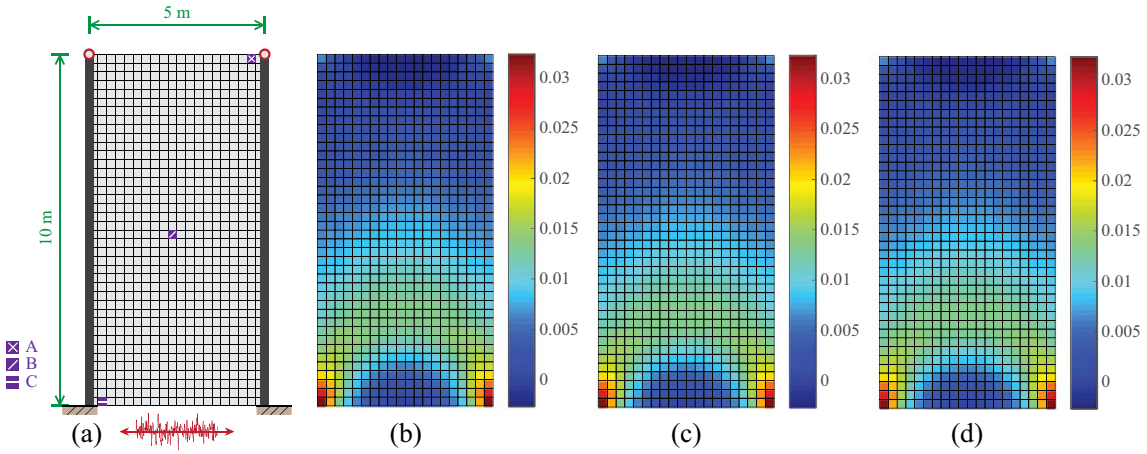

Fig. 3 Sensitivities by different approaches: (**a**) geometry of the structure, (**b**) adjoint method, (**c**) direct differentiation method, and (**d**) finite difference method

average tip-displacement exceeds a given threshold value u_0(=0.02 m) at t_0=8, i.e.

$$E_f = u_0 - \left(\frac{u_{Left} + u_{Right}}{2}\right) \leq 0 \tag{46}$$

where $u_{Left} = \mathbf{a}(t_0, \tilde{\boldsymbol{\rho}})_{Left}^{\mathrm{T}}\mathbf{v}$ and $u_{Right} = \mathbf{a}(t_0, \tilde{\boldsymbol{\rho}})_{Right}^{\mathrm{T}}\mathbf{v}$ denote displacements at time t_0 respectively, computed using $\mathbf{a}(t_0, \tilde{\boldsymbol{\rho}})$ functions evaluated at the left and right red dots in Fig. 3(a), respectively. The direct differentiation method (DDM) and the proposed adjoint method (AJM) are carried out to calculate the sensitivity $\partial\beta(u_0 = 0.02, t_0 = 8, \tilde{\boldsymbol{\rho}})/\partial d_j$. The finite difference method (FDM) with varying perturbations from Δd=10^{-1} to Δd=10^{-16} is also implemented to verify the proposed method. Table 1 summarizes sensitivity results from the FDM at three selected elements shown in Fig. 3(a) and those from the proposed AJM and the DDM. Figure 3 (b)-(d) show normalized sensitivities computed by the three methods. The DDM and proposed AJM yield results that are

Table 1 Sensitivities at the element A, B, and C using the proposed AJM, DDM, and FDM with a perturbation Δd

	Elem. A	Elem. B	Elem. C				
AJM	0.003110	0.008650	0.021623				
DDM	0.003110	0.008650	0.021623				
FDM							
Δd	Elem. A	Elem. B	Elem. C	Δd	Elem. A	Elem. B	Elem. C
1×10^{-1}	0.002585	0.007872	0.020308	1×10^{-9}	0.003361	0.008789	0.022355
1×10^{-2}	0.003053	0.008570	0.021484	1×10^{-10}	0.018385	0.018541	0.029197
1×10^{-3}	0.003104	0.008642	0.021609	1×10^{-11}	0.159606	0.143707	0.081490
1×10^{-4}	0.003109	0.008650	0.021621	1×10^{-12}	0.311751	-0.32685	0.567768
1×10^{-5}	0.003110	0.008650	0.021623	1×10^{-13}	13.37375	9.74998	5.90417
1×10^{-6}	0.003112	0.008652	0.021624	1×10^{-14}	85.7980	242.6503	71.7870
1×10^{-7}	0.003128	0.008635	0.021620	1×10^{-15}	-1345.81	206.501	315.525
1×10^{-8}	0.002872	0.008645	0.021704	1×10^{-16}	1725.286	4276.579	11146.63

consistent with those from the FDM. Figure 4 shows normalized computational times for different levels of discretization of the structure. The computational times are normalized by the result of the AJM for 800 finite elements. The proposed AJM shows the most efficient performance in terms of computational time while maintaining the accuracy of results.

5 Numerical applications

The proposed method is applied to obtain a lateral bracing system with minimum volume for a building structure subjected to stochastic ground motion excitations. The topology optimization formulation in (25) is used while the objective function $f_{obj}(\tilde{\boldsymbol{\rho}}(\mathbf{d}))$ is defined as the volume of the structure determined by the material density distribution. The material distribution in the design domain is optimized under probabilistic constraints on inter-story drift ratios (ASCE7 2010, NEHRP 2009) during random excitations of an earthquake event, which are important criteria for seismic designs. Topology optimization is performed for a variety of multi-story buildings and conditions in order to investigate the impact of prescribed probabilistic parameters, characteristics of the filtered white noise, and building dimensions on topology optimization solutions.

5.1 Input stochastic process

In subsequent numerical examples presented in this paper, the stochastic seismic excitation is modeled as the filtered white-noise process. Accordingly, the unit-impulse response function $h_f(\cdot)$ in (7) follows the Kanai-Tajimi filter model (Clough and Penzien 1993; Fujimura and Der Kiureghian 2007), i.e.

$$h_f(t) = \exp(-\zeta_f \omega_f t)\left[\frac{\left(2\zeta_f^2-1\right)\omega_f}{\sqrt{1-\zeta_f^2}}\sin\left(\omega_f\sqrt{1-\zeta_f^2}\cdot t\right)-2\zeta_f\omega_f\cos\left(\omega_f\sqrt{1-\zeta_f^2}\cdot t\right)\right] \tag{47}$$

where ω_f and ζ_f are filter parameters representing the predominant frequency and the bandwidth of the process. The corresponding power spectral density (PSD) function (Lutes and Sarkani 2003) of the input process is

$$\Phi(\omega) = \frac{1+4\zeta_f^2\left(\omega/\omega_g\right)^2}{\left(1-\left(\omega/\omega_g\right)^2\right)^2+\left(2\zeta_f\omega/\omega_g\right)^2}\Phi_0 \tag{48}$$

where Φ_0 represents the power spectral density of the underlying white noise process. Typical values for predominant frequency and the bandwidth of ground motions on a firm ground are $\omega_f = 5\pi$ rad/s and $\zeta_f = 0.4$.

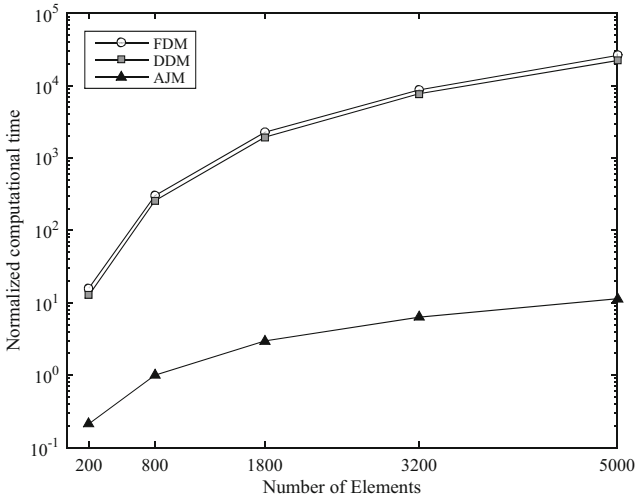

Fig. 4 Normalized computational time (FDM: finite difference method, DDM: direct differentiation method, and AJM: adjoint method)

5.2 Topology optimization of three-story buildings

Figure 5 shows a three-story building with a width of 5 m, a height of 15 m, and a uniform thickness of 0.1 m. The design domain, represented by the gray area, is modeled by bilinear quadrilateral (Q4) elements, and the material densities in the elements are optimized to minimize the volume while satisfying the probabilistic constraints on the inter-story drift ratio. The two vertical lines represent the structural columns modeled by frame elements, whose material properties or dimensions remain constant during the optimization process. The frame element is discretized into many smaller frame elements, which are attached at every node of quadrilateral meshes along the column lines and move together with quadrilateral elements. Young's modulus E=21,000 MPa and density ρ=2,400 kg/m^3 are used as material properties to represent normal-weight concrete. The filtering radius r=0.1625 m and initial volume fraction 0.7 over the Q4 domain are employed. The coefficients used in the Rayleigh damping model are κ_0= 1.93, $\kappa_1 = 1.52\times10^{-4}$ under the assumption of 2 % damping ratio for the three-story building. For each of the floor levels 2, 3 and 4 shown in Fig. 5, the averages of the inter-story drift ratios (Δ_i/L_i) are evaluated at specified points for the left and right columns as the stochastic response of the structure. Constraints are given on the probabilities of the failure events, which are defined as those exceeding the average inter-story drift ratios for the given threshold value. More precisely, the failure event of the i-th floor level is defined as

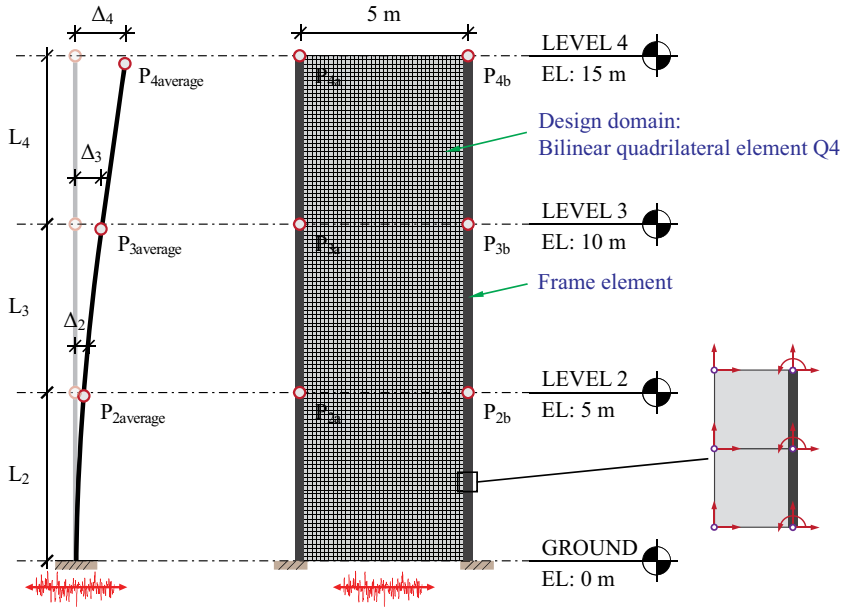

Fig. 5 Three-story building subjected to stochastic excitations

$$E_{f_i} = \left\{ u_{i0} - \left(\frac{\left(\mathbf{a}(t_0,\tilde{\boldsymbol{\rho}})^{\mathrm{T}}_{i,Left} + \mathbf{a}(t_0,\tilde{\boldsymbol{\rho}})^{\mathrm{T}}_{i,Right}\right)\mathbf{v}}{2L_i} \right) \le 0 \right\} \quad \text{for } i = 2$$

$$\left\{ u_{i0} - \left(\frac{\left(\mathbf{a}(t_0,\tilde{\boldsymbol{\rho}})^{\mathrm{T}}_{i,Left} + \mathbf{a}(t_0,\tilde{\boldsymbol{\rho}})^{\mathrm{T}}_{i,Right}\right)\mathbf{v}}{2L_i} - \frac{\left(\mathbf{a}(t_0,\tilde{\boldsymbol{\rho}})^{\mathrm{T}}_{(i-1),Left} + \mathbf{a}(t_0,\tilde{\boldsymbol{\rho}})^{\mathrm{T}}_{(i-1),Right}\right)\mathbf{v}}{2L_i} \right) \le 0 \right\} \quad \text{for } i = 3,4 \tag{49}$$

where L_i(=5 m), u_{i0}(=0.02), $\mathbf{a}(t_0,\tilde{\boldsymbol{\rho}})^{\mathrm{T}}_{i,Left}$ and $\mathbf{a}(t_0,\tilde{\boldsymbol{\rho}})^{\mathrm{T}}_{i,Right}$ represent the floor height, the threshold value of the inter-story drift ratio respectively, as well as **a** vectors to determine the lateral displacement at the left and right columns of the i-th floor level at $t=t_0$, for i=2,3,4. Although the events described in (49) have a different form from (26), it is noted that the inter-story drift ratios in (49) are still linear functions of the random vector **v**, i.e. $\mathbf{b}(t_0,\tilde{\boldsymbol{\rho}})^{\mathrm{T}}_i\mathbf{v}$. Therefore, the closed-form solution in (27) and the sensitivity calculation methods developed in Section 4.1 can still be used by replacing **a** vectors (displacement) in the formulations by **b** vector (inter-story drift). Table 2 provides filter parameters, column size, and parameters used for probabilistic constraints, which include the threshold values of average drift ratios. The filter parameters in Table 2 represent ground motions on a typical firm ground. The threshold value of the inter-story drift ratio is chosen as one of design criteria in ASCE7 (2010).

Table 2 Three-story building: parameters used for design domain, probabilistic constraint and ground motion model

	Filter parameters		Column size (m×m)	u_0
	ω_f	ζ_f		
Case I	5π	0.4	0.5×0.5	0.02
Case II	5π	0.4	0.5×0.5	0.0175
Case III	5π	0.4	0.6×0.6	0.02

In these examples, constraints are given on the instantaneous probability during the strong ground motions for which the earthquake excitation can be approximated as a stationary process (Soong & Grigoriu 1993). Even when a stationary input is used for a linear structure, it takes time to achieve the stationarity in the structural response. In order to achieve stationarity, the drift ratio at t_0=6 s is used when computing the instantaneous failure probability. Optimization problems are solved with different column sizes, intensities of filtered Gaussian excitations, and target reliability indices, which correspond to allowable failure probabilities.

Topology optimization solutions are obtained (see Figs. 6 and 7) while the intensity of the ground motion is varied for Cases I-III as tabulated in Table 2. As the intensity increases,

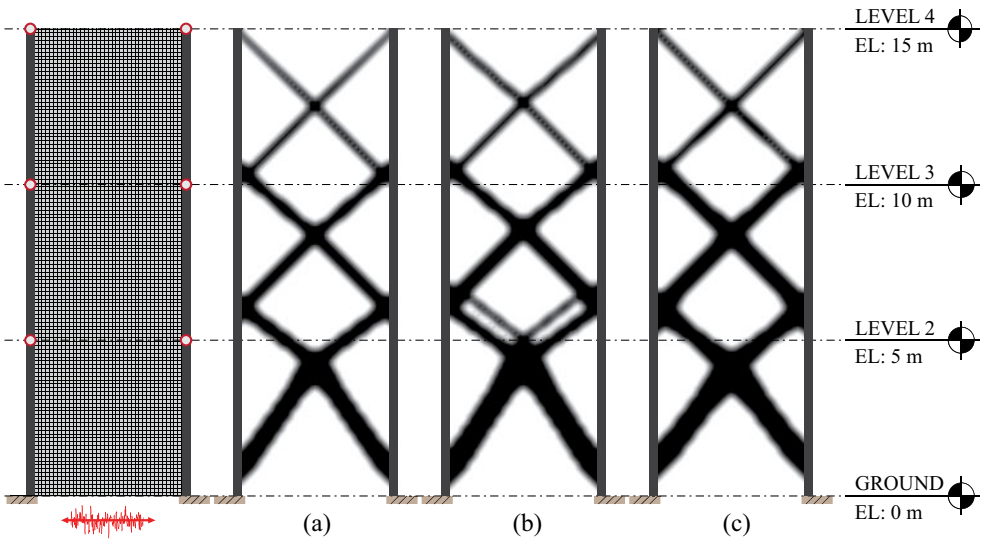

Fig. 6 Topology optimization solutions to the three-story building example (Φ_0=250, β^{target}=2.5, P_f=0.62 %). (**a**) Case I: column size 0.5 m×0.5 m, u_0 =0.02; (**b**) Case II: column size 0.5 m × 0.5 m, u_0 =0.0175; (**c**) Case III: column size 0.6 m×0.6 m, u_0 =0.02

the converged topologies become significantly different at the lower level. In particular, the intersection point of the bracing at the lower level moves up vertically with increasing intensity while the thickness of the bracing increases at the lower level but remains relatively stable at higher levels. The results shown in Figs. 6 and 7 indicate that topology optimization satisfies probabilistic constraints for increased intensities by strengthening the lower level first, i.e. by placing more materials and changing geometry of the bracings. This is why the bracing of the top level mostly remains constant and maintains its 45° angle as the intensity increases. It is also noted that the points where the bracing meets the column around the second floor (termed as "bracing-column points" hereafter) move up as the intensity increases. Based on this observation, an efficient way to control the inter-story drift ratio is strengthening lower parts of the structural system. Comparing results from Case I and Case II shows that decreased threshold value of drift ratios (Case II) moves up both bracing-column points and intersection points of the bracings at the lower floor level. It is also important to note that a change in the threshold value can affect the optimization result as shown in both Case I and Case II. Distinct changes of topologies are observed at the lower floor level with additional branches of the material distribution for the case with reduced threshold value. The change in the column size (Case III) leads to overall increases in the thickness of material distributions. Volumes of the optimization solutions are tabulated in Table 3. The values in the parentheses are volumes for discrete material distributions converted from intermediate densities. Detailed discussion of the conversion process and its impact on the results are included in Section 5.3. The volumes of optimization solutions for Case I are lower than those of Case II because the

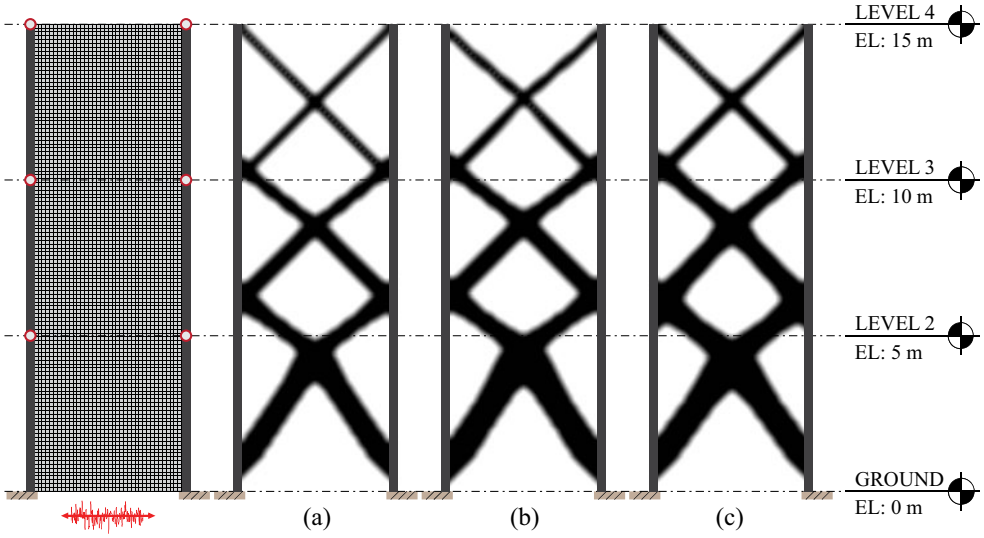

Fig. 7 Topology optimization solutions to the three-story building example (Φ_0=300, β^{target}=2.5, P_f=0.62 %). (**a**) Case I: column size 0.5 m×0.5 m, u_0 =0.02; (**b**) Case II: column size 0.5 m×0.5 m, u_0 =0.0175; (**c**) Case III: column size 0.6 m × 0.6 m, u_0 =0.02

Table 3 Volume of final topologies (β^{target}=2.5, P_f=0.62 %)

Φ_o	Case I	Case II	Case III
250	1.717 (1.734) m^3	2.049 (2.059) m^3	2.157 (2.169) m^3
300	1.904 (1.928) m^3	2.251 (2.278) m^3	2.402 (2.419) m^3

lower threshold values of inter-story drift ratios in Case I requires more strict the constraints. Compared to Case I, the larger column size in Case III results in the increased optimized volume. Note that the column size does not change during topology optimization, and thus the stiffness and mass matrices of the column remain the same. Therefore, in Case III, applied earthquake loads to degrees of freedom along column locations would be greater than dynamic forces applied to columns in Case I, resulting in the increased volume.

The target reliability index of the cases is changed to 2.0 and 3.0 which correspond to the target failure probabilities $P_f^{target}=\Phi[-2.0]=2.28$ % and $P_f^{target}=\Phi[-3.0]=0.13$ %, respectively. The optimization solutions using changed target reliability indices are illustrated in Figs. 8 and 9. This shows the impact of changing the target reliability index on optimal bracings. More specifically, the increase in the reliability index results in thicker bracings and alters intersection points on the first two bottom floor levels. Additional branches of material distributions are also observed and the volumes obtained for the cases in Figs. 8 and 9 are summarized in Table 4.

Figure 10 shows the convergence histories of the objective function (volume), the reliability index and the failure probability of Case II shown in Fig. 9 (b), whose parameters are Φ_0=300, β^{target}=3.0, u_0=0.0175. The convergence histories confirm that the proposed topology optimization method and the sensitivity formulation can successfully achieve the topology optimization solution under constraints on the instantaneous failure probabilities defined in terms of the drift ratios. Additionally, a neighborhood in the design domain that satisfies the constraints is quickly identified, and the remaining design iterations are to achieve the minimum volume within the identified neighborhood. Figure 11 shows time histories of inter-story drift ratios (Case II, Φ_0=300, β^{target}=3.0, u_0=0.0175) of the initial design (i.e. the continuum domain completely filled) and the optimal design for an input process randomly generated from the Kanai-Tajimi filter model. The optimized system shows improved dynamic performance even though only 40.1 % of the original volume is used.

A manufacturing constraint on pattern repetition in topology optimization (Almeida et al. 2010; Stromberg et al. 2011) can be implemented for practical engineering applications. This constraint allows engineers to achieve constructability of the structural system such as same connection details, reusages of formworks for bracing and considering aesthetic perspective as well. Topology optimization results of Case I with β^{target}=2.5, and varying Φ_0 of 250 or 300 are shown in Figs. 12 and 13. The number of pattern repetitions m=2, 3 and 4 are used to obtain these results. Volumes of topology optimization results are summarized in Table 5.

5.3 Study of stochastic responses over topology optimization results

After the topology optimization result is obtained with the constraint on the instantaneous failure probability at the time point t_0=6 s, reliability indices and failure probabilities of the obtained topology layout solution at different time points from 0.5 s to 10 s are studied. For this study, the topology optimization result with the pattern repetition shown in Fig. 13 (c) is used. Our results show that failure probabilities (and reliability indices) remain constant within the time duration considered after approximately 3 s (see Fig. 14). This confirms that the

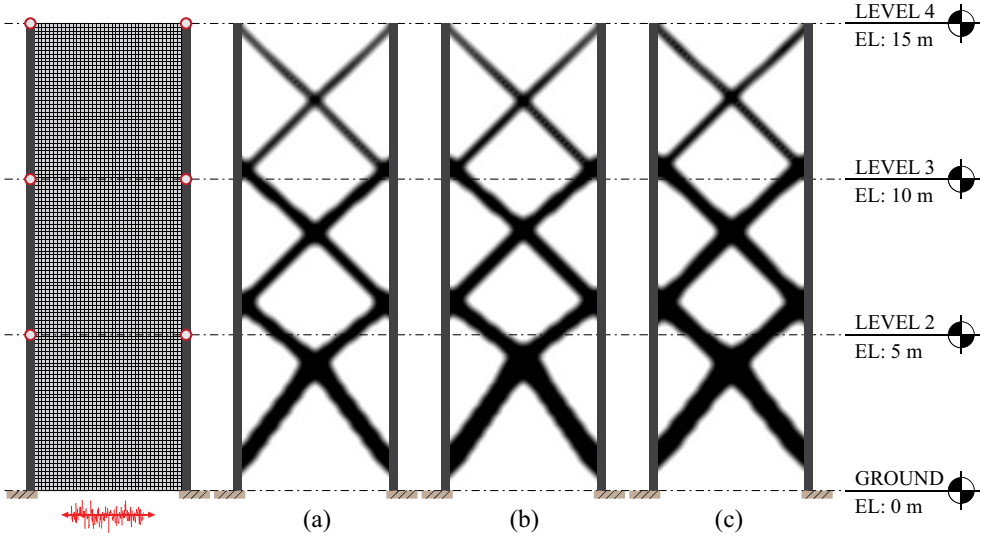

Fig. 8 Topology optimization solutions to the three-story building example (Φ_0=300, β^{target}=2.0, P_f=2.28 %). (**a**) Case I: column size 0.5 m×0.5 m, u_0 =0.02; (**b**) Case II: column size 0.5 m×0.5 m, u_0 =0.0175; (**c**) Case III: column size 0.6 m×0.6 m, u_0 =0.02

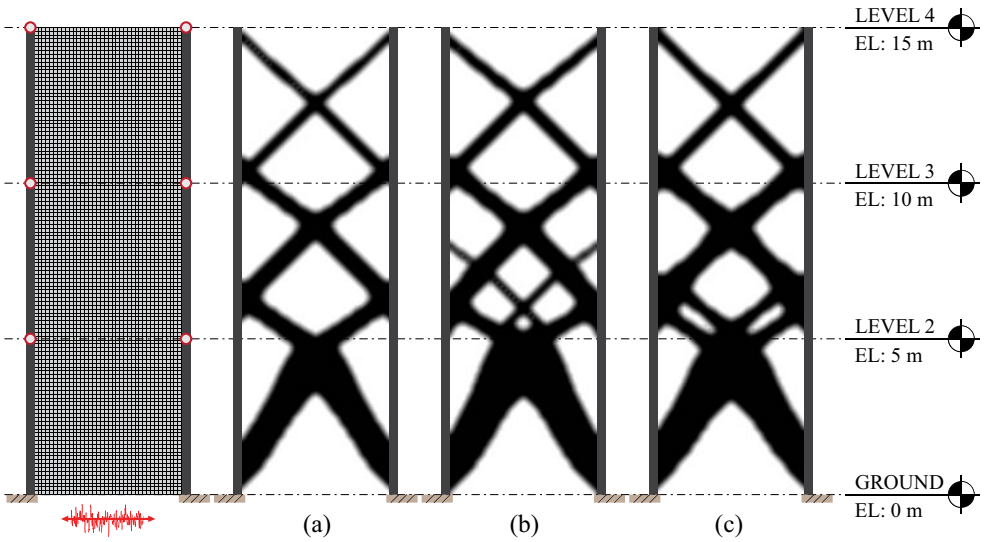

Fig. 9 Topology optimization solutions to the three-story building example (Φ_0=300, β^{target}=3.0, P_f=0.13 %). (**a**) Case I: column size 0.5 m×0.5 m, u_0 =0.02; (**b**) Case II: column size 0.5 m×0.5 m, u_0 =0.0175; (**c**) Case III: column size 0.6 m x 0.6 m, u_0 =0.02

optimization solution at the specific time point (t_0=6 s) by the proposed method under the filtered Gaussian input process can represent the reliability of the system during the stationary strong motion period.

The effects of solutions converted to discrete material layouts on dynamic responses and failure probabilities are studied for practical engineering purposes. During a post-processing stage, material densities less than 0.5 are converted to zero, and those that are greater than 0.5 are converted to one. The optimization results under the pattern repetition constraint (see Figs. 12 and 13) are processed using converted material densities. The layout solutions of this process are illustrated in Figs. 15 and 16. Comparison of results between continuous solutions in Figs. 12 and 13 and interpreted discrete solutions after the post-processing are tabulated in Table 6. Discrete solutions show increased reliability indices in all cases and result in lower failure probabilities. Dynamic responses of the continuous solution of Φ_0=300, β^{target}=2.5, and m=4 (see Fig. 13 (c)) in each floor level and the discrete solution (see Fig. 16 (c)) under a randomly generated filtered ground motion are shown in Fig. 17. Compared to the continuous solutions, the overall dynamic responses of the discrete layout solution show reduced magnitudes, which indicate the possibility of the lower failure probability.

Table 4 Volume of final topologies (Φ_0=300)

β^{target}	Case I	Case II	Case III
2.0	1.505 (1.531) m^3	1.720 (1.731) m^3	1.870 (1.884) m^3
3.0	2.401 (2.409) m^3	3.004 (3.022) m^3	3.077 (3.100) m^3

Lastly, a cross-comparison among optimization results is performed to study whether different model parameters in topology optimization lead to significant changes of structural responses. As shown in Fig. 18, differences in dynamic responses of Case I and Case III under Φ_0=250, β^{target}=2.5 are negligible. The topology optimization result of Case II, which has u_0 = 0.0175 leads to overall reduced magnitude compared to others, resulting in observable differences in structural responses. Further study of optimization solutions from the pattern repetition constraint was performed. Figure 19 illustrates structural responses of topology optimization results subjected to a randomly generated ground motion with Φ_0=300, β^{target}=2.5, P_f=0.62 % considered in Fig. 16 (a)-(c) with the number of pattern repetitions m. Structural responses of these cases remain relatively constant despite changes in pattern numbers, which led to different material layouts and final volumes.

5.4 Study of geometric uncertainty of discrete material distribution

A further study on the geometry uncertainty is carried out. The geometry uncertainty may be caused during the converting process in practical fields from continuous topology optimization solutions to discrete ones aforementioned in Section 5.3. Thus, the cut-off value of material density assumes that it follows the normal distribution with a mean of $\mu_{m\_cut\text{-}off}$ and a standard deviation of $]\sigma_{cut\text{-}off}$ rather than the fixed value 0.5. Therefore, each density value in each finite element is compared to a random cut-off value in order to convert to discrete material layouts. Figure 20 shows discrete solutions of Case III (Φ_0=250, β^{target}=2.5) shown in Fig. 16 (c) under the geometry

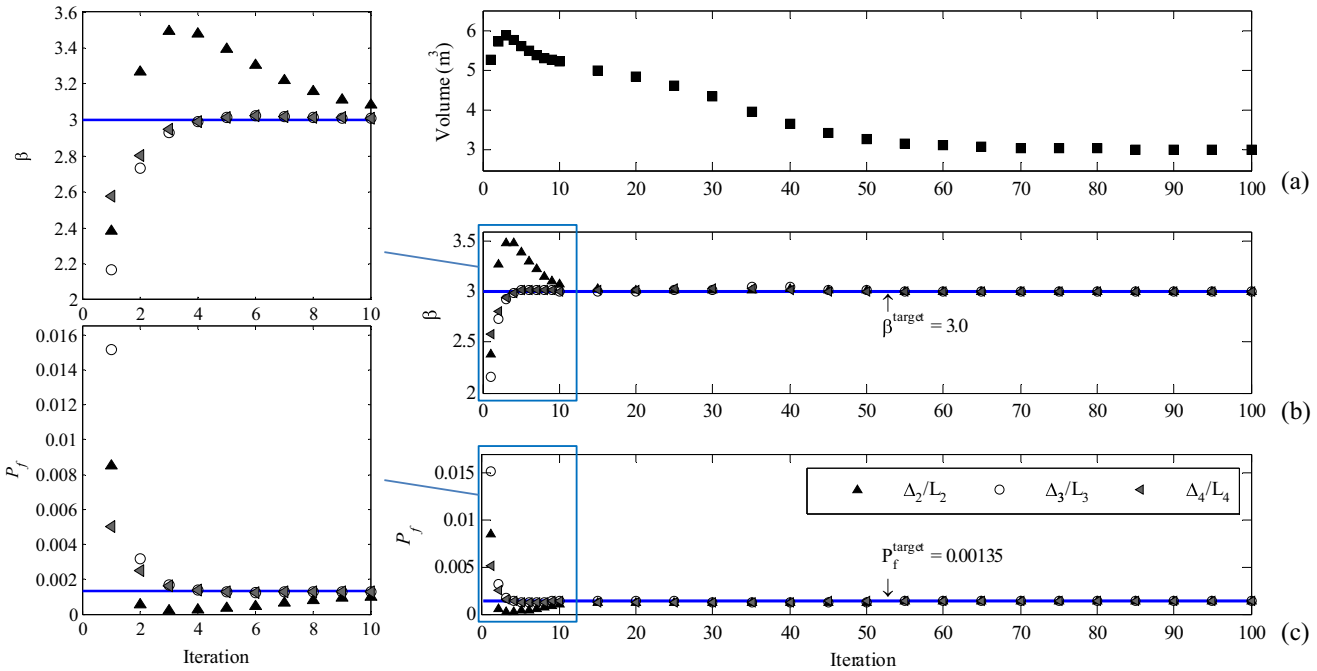

Fig. 10 Convergence history of the problem shown in Fig. 9 (b): (**a**) volume (**b**) reliability index (**c**) failure probability

uncertainty. It is noted that the result is one of 20 simulations with random cut-offs. A discrete solution without the geometry uncertainty is provided in Fig. 20 (a) for comparison. Figure 21 shows effects of geometry uncertainties on reliability indices associated with inter-story drift ratio constraints after 20 simulations. The reliability indices are still within target reliability indices from continuous solutions and reliability indices from discrete solutions.

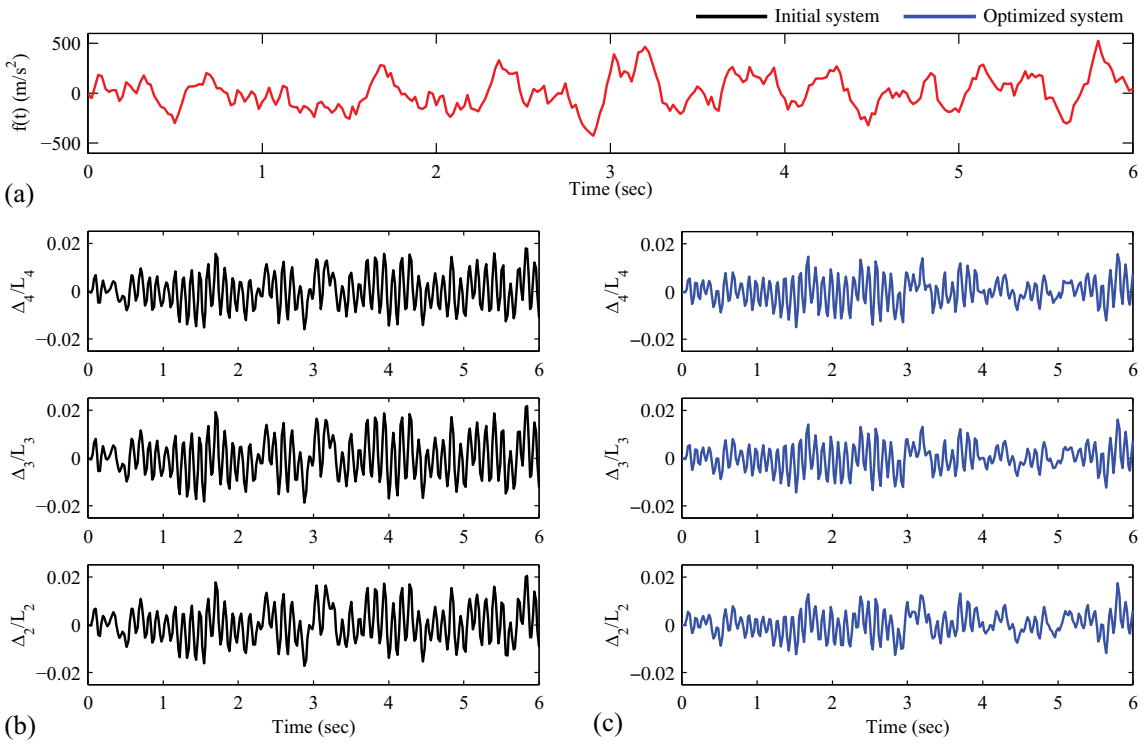

Fig. 11 Dynamic response comparison of the problem shown in Fig. 9 (b): **(a)** Randomly generated ground motion excitations; **(b-c)** corresponding dynamic responses of the initial design and the optimal design

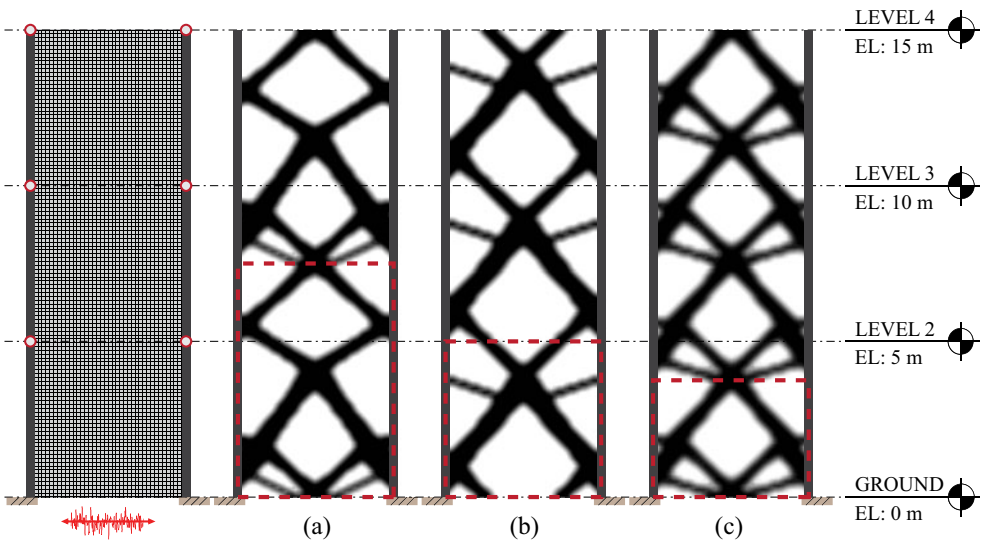

Fig. 12 Topology optimization solutions to the three-story building example with the pattern repetition constraint. Φ_0=250, β^{target}=2.5, P_f=0.62 %: (**a**) m=2; (**b**) m=3; (**c**) m=4

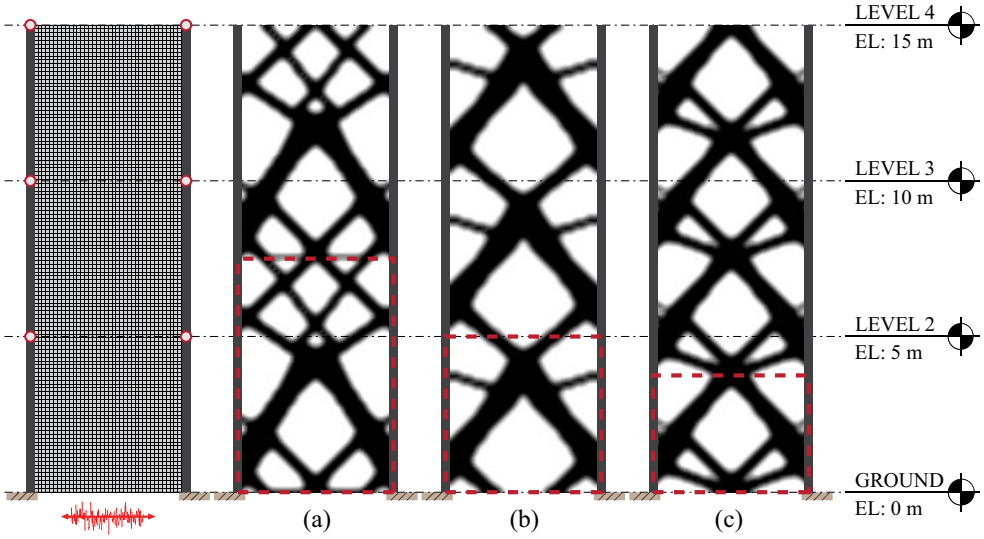

Fig. 13 Topology optimization solutions to the three-story building example with the pattern repetition constraint. Φ_0=300, β^{target}=2.5, P_f=0.62 %: (**a**) m=2; (**b**) m=3; (**c**) m=4

5.5 Parametric study on impact of ground motion characteristics

A numerical example of a six-story building is considered for a parametric study on the impact of ground motion characteristics. The example employs the same parameters as those used for the three-story building example unless specified otherwise. Coefficients κ_0=0.56 and κ_1=5.0×10^{-4} are used for the Rayleigh damping model to achieve 2 % damping. The column sizes and the target reliability indices are shown in Table 7.

Table 5 Volume of final topologies with the pattern repetition constraint (β^{target}=2.5, P_f=0.62 %)

Φ_0	m=2	m=3	m=4
250	2.627 (2.656) m^3	2.590 (2.616) m^3	2.995 (3.037) m^3
300	3.117 (3.144) m^3	2.966 (3.001) m^3	3.318 (3.363) m^3

Three values of the dominant frequency and damping ratio (bandwidth) of the Kanai-Tajimi filter are applied respectively, i.e. ω_f=4.7π, 5.0 π, 5.3 π (rad/sec) and ζ_f=0.2, 0.3, 0.4. The impact of the dominant frequency is shown in Fig. 22 (a)-(c), while Fig. 22 (d)-(e) demonstrates the impact of the bandwidth parameter. The convergence history of volumes for different parameters in damping ratios and dominant frequencies are shown in Fig. 23. From the modal analysis of the original

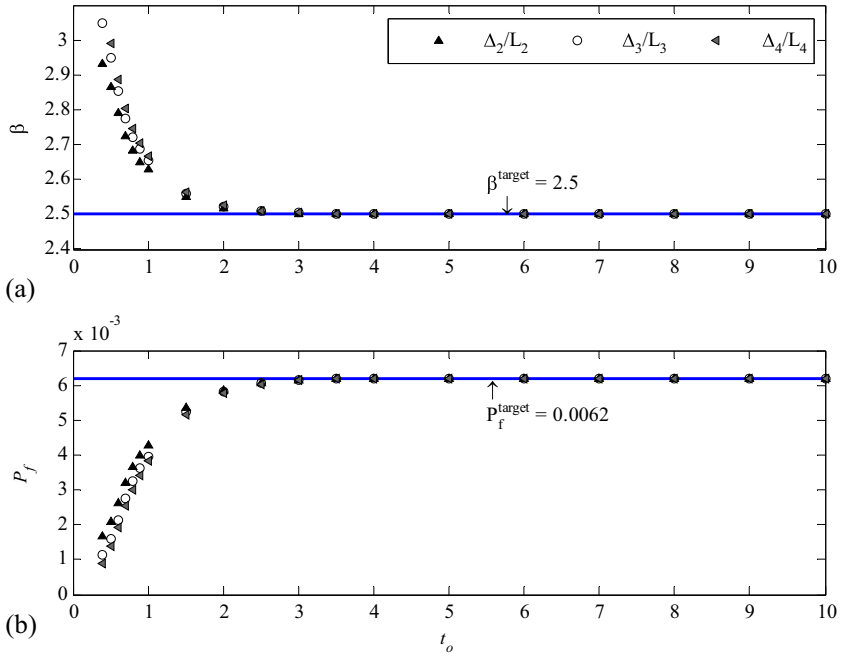

Fig. 14 (**a**) Reliability index and (**b**) failure probability of the topology optimization solution in Fig. 13 (c) with varying time points

structure with the uniform distribution of the material density 0.5 over the Q4 design domain, the first natural frequency of the six-story building is approximately 18.06 rad/s (the natural period T_1 =0.348 s). A decrease in the damping ratio of the filter (the bandwidth of the process) increases the optimized volume, as shown in Fig. 23. In order to identify the causes for these results, the power spectral density function of the input ground motion is plotted in Fig. 24 (a). For the given ground motion model, a decrease in the filter damping ratio increases the power spectral density at the natural frequency of the building structure, which explains the increase in the volume of the optimization solution. Figure 24 (b) shows that an increase in the predominant frequency of the filter increases the power spectral density at the natural frequency. This shows why an increase in the dominant frequency results in larger optimized volume for the given example, as shown in Fig. 23.

It is observed that characteristics of the ground motion make significant impacts on the topologies such as geometries, intersection points, bracing-column points, and the shape of the bracings. Additionally, the match between the frequency content of the ground motion

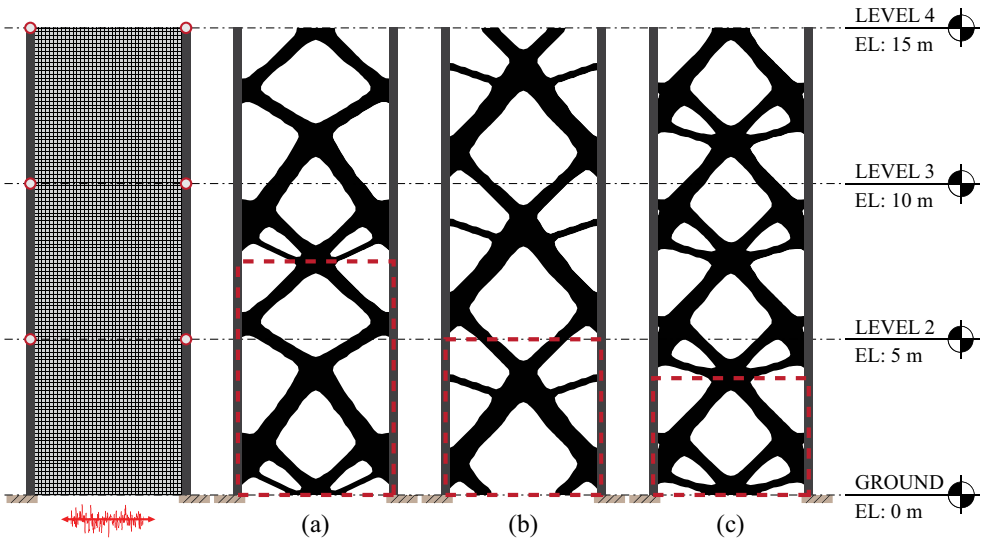

Fig. 15 Discrete solutions to the three-story building example with the pattern repetition constraint. Φ_0=250, β^{target}=2.5, P_f=0.62 %: (**a**) m=2; (**b**) m=3; (**c**) m=4

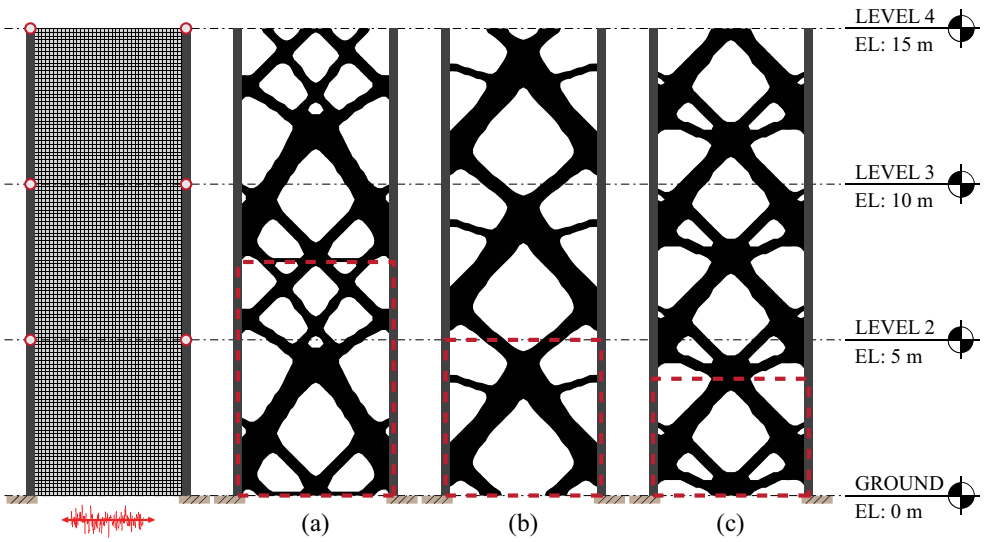

Fig. 16 Discrete solutions to the three-story building example with the pattern repetition constraint. Φ_0=300, β^{target}=2.5, P_f=0.62 %: (**a**) m=2; (**b**) m=3; (**c**) m=4

Table 6 Comparison between continuous solution and discrete solution (β^{target}=2.5, P_f=0.62 %)

	Continuous solution		Discrete solution											
			Φ_0=250						Φ_0=300					
			m=2	m=3	m=4	m=2	m=3	m=4	m=2	m=3	m=4	m=2	m=3	m=4
	β	P_f	β			P_f			β			P_f		
E_{f_1}	2.5	0.621	2.83	2.88	2.97	0.233	0.199	0.149	2.83	2.82	2.91	0.233	0.240	0.181
E_{f_2}	2.5	0.621	2.89	2.80	2.87	0.193	0.256	0.205	2.88	2.73	2.79	0.199	0.317	0.264
E_{f_3}	2.5	0.621	2.72	2.89	2.77	0.326	0.193	0.280	2.77	2.79	2.83	0.280	0.264	0.233

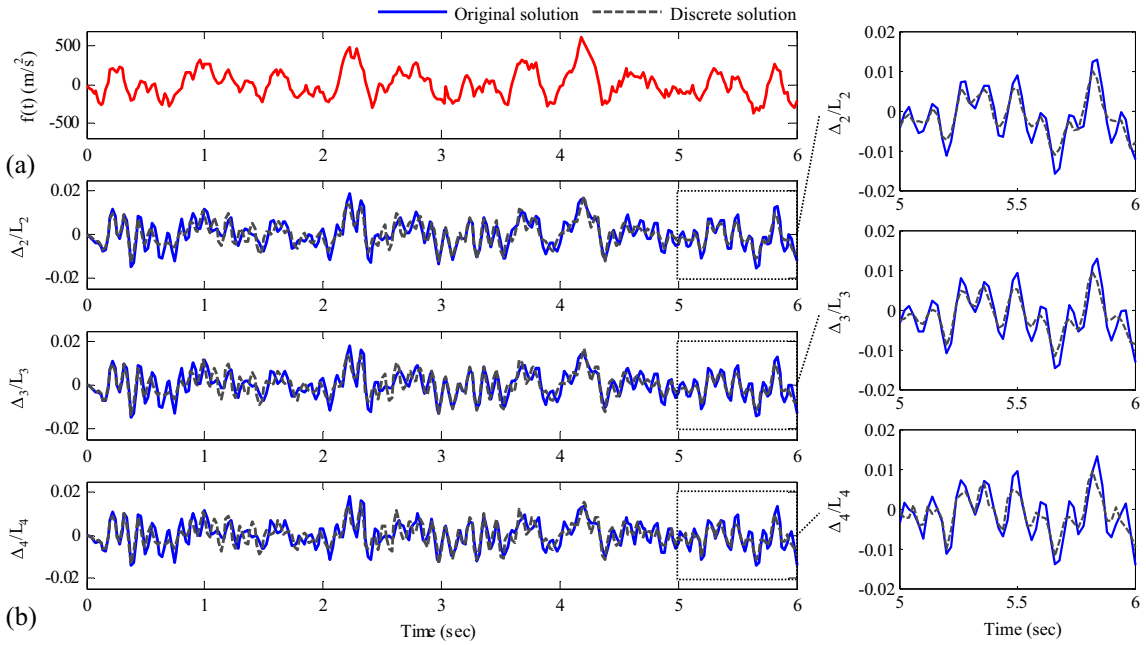

Fig. 17 Dynamic response comparison between continuous solution shown in Fig. 13 (c) and discrete solution of Fig. 16 (c). Randomly generated ground motion excitations (**a**) and corresponding dynamic responses (**b**)

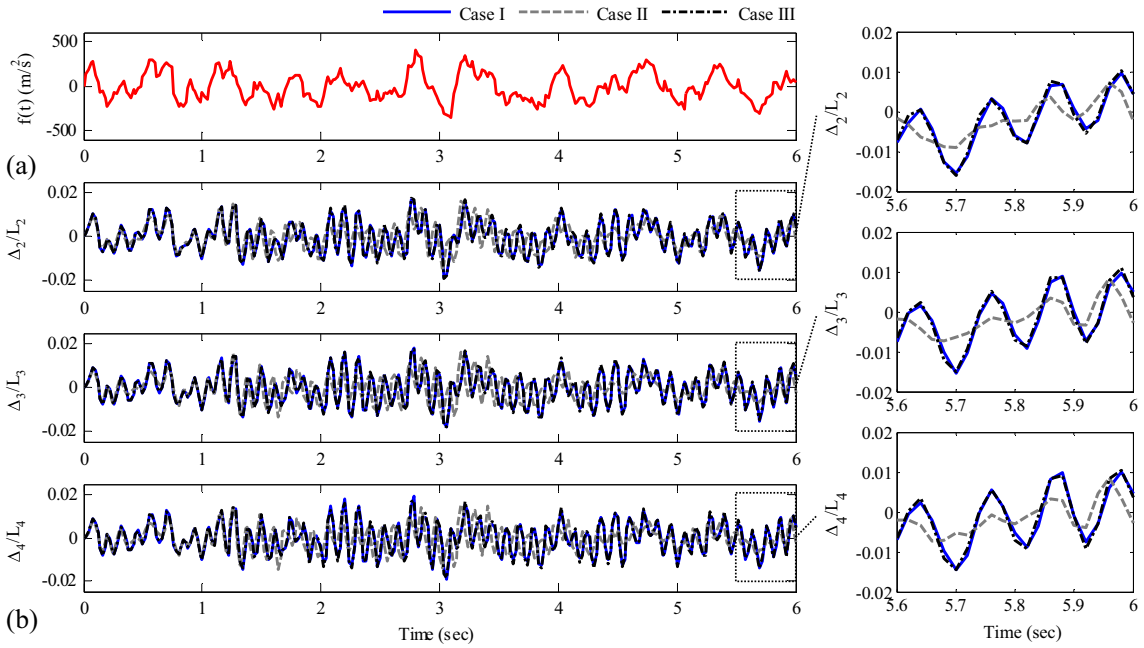

Fig. 18 Comparison of topology optimization results to the three-story building example, Φ_0=250, β^{target}=2.5, P_f=0.62 %. Randomly generated ground motion excitations (**a**) and corresponding dynamic responses (**b**). (Case I: column size 0.5 m×0.5 m, u_0 =0.02. Case II: column size 0.5 m×0.5 m, u_0 =0.0175. Case III: column size 0.6 m×0.6 m, u_0 =0.02)

and the natural frequency of the structure affects how the ground motion characteristics determine topological solutions. Therefore, it is important to describe the frequency content of the ground motion accurately during topology optimization under stochastic excitations.

The pattern repetition constraint of the aforementioned example of three story building is further applied to the six story building problem. Figure 25 shows topology optimization solutions for the number of patterns under two target reliability indices β^{target}=2.5 and

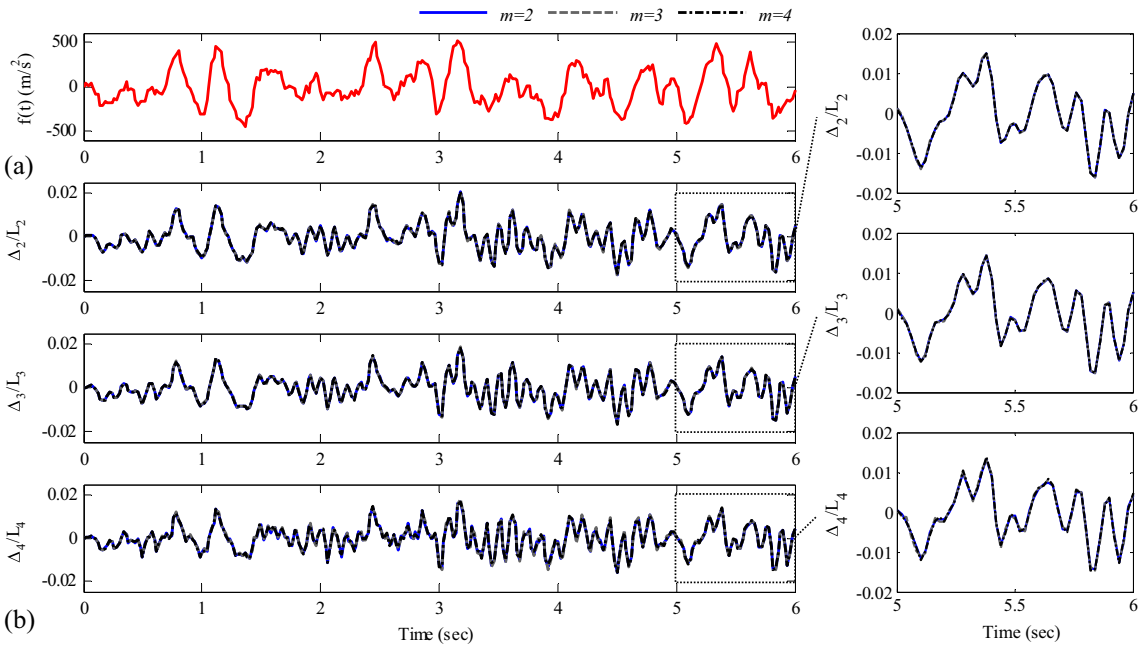

Fig. 19 Comparison of topology optimization results to the three-story building example with the pattern repetition constraint, Φ_0=300, β^{target}=2.5, P_f= 0.62 %. Randomly generated ground motion excitations (**a**) and corresponding dynamic responses (**b**)

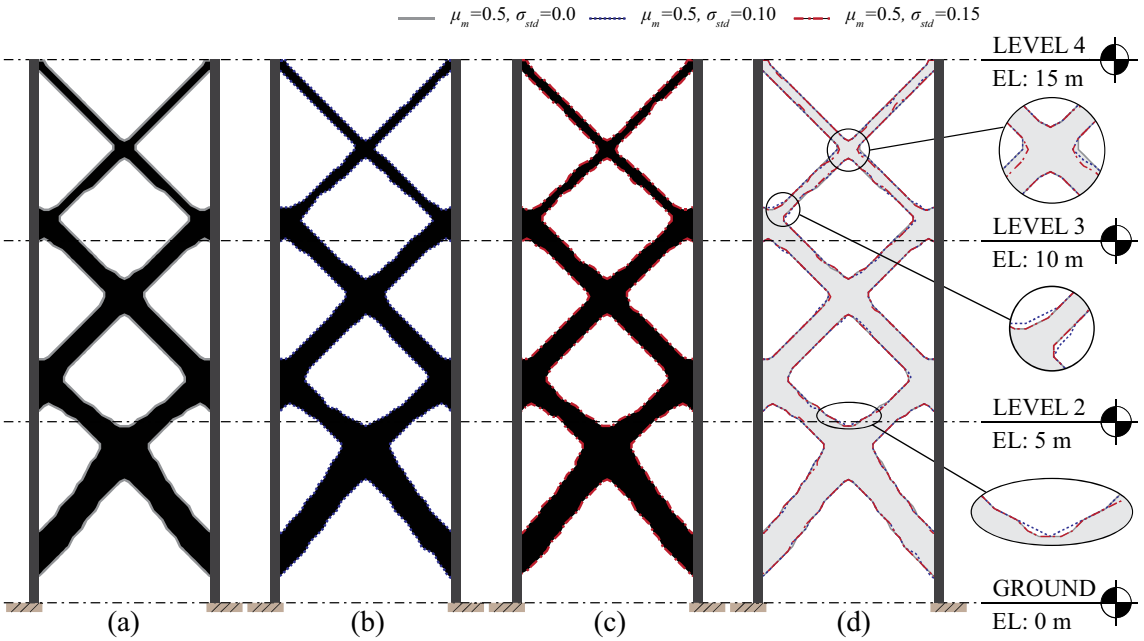

Fig. 20 Discrete solutions under geometry uncertainty: (**a**) $\mu_{m\_cut\text{-}off}$=0.5, $\sigma_{cut\text{-}off}$=0; (**b**) $\mu_{m\_cut\text{-}off}$=0.5, $\sigma_{cut\text{-}off}$=0.1; (**c**) $\mu_{m\_cut\text{-}off}$=0.5, $\sigma_{cut\text{-}off}$=0.15; (**d**) overlapped outlines of Fig. 20 (a)-(c)

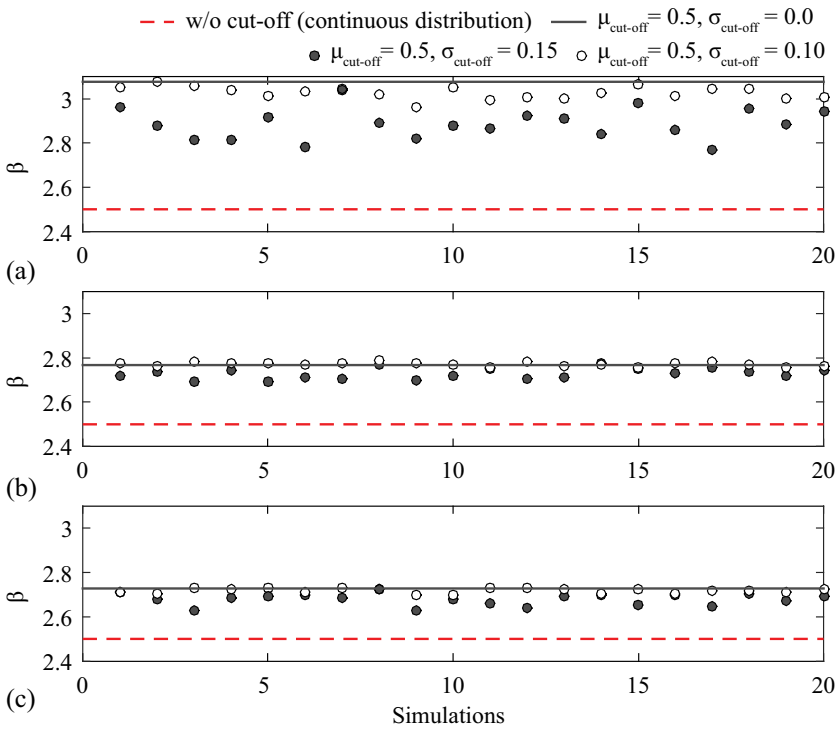

Fig. 21 Reliability indices associated inter-story drift ratio constraints after geometry uncertainty simulations. (**a**) Δ_4/L_4; (**b**) Δ_3/L_3; (**c**) Δ_2/L_2

Table 7 Six-story building: Parameters used for design domain, probabilistic constraint and ground motion model

Φ_0	β^{target}	P_f^{target} (%)	Column size (m×m)	u_0
2	2.5	0.62	0.6×0.6	0.02

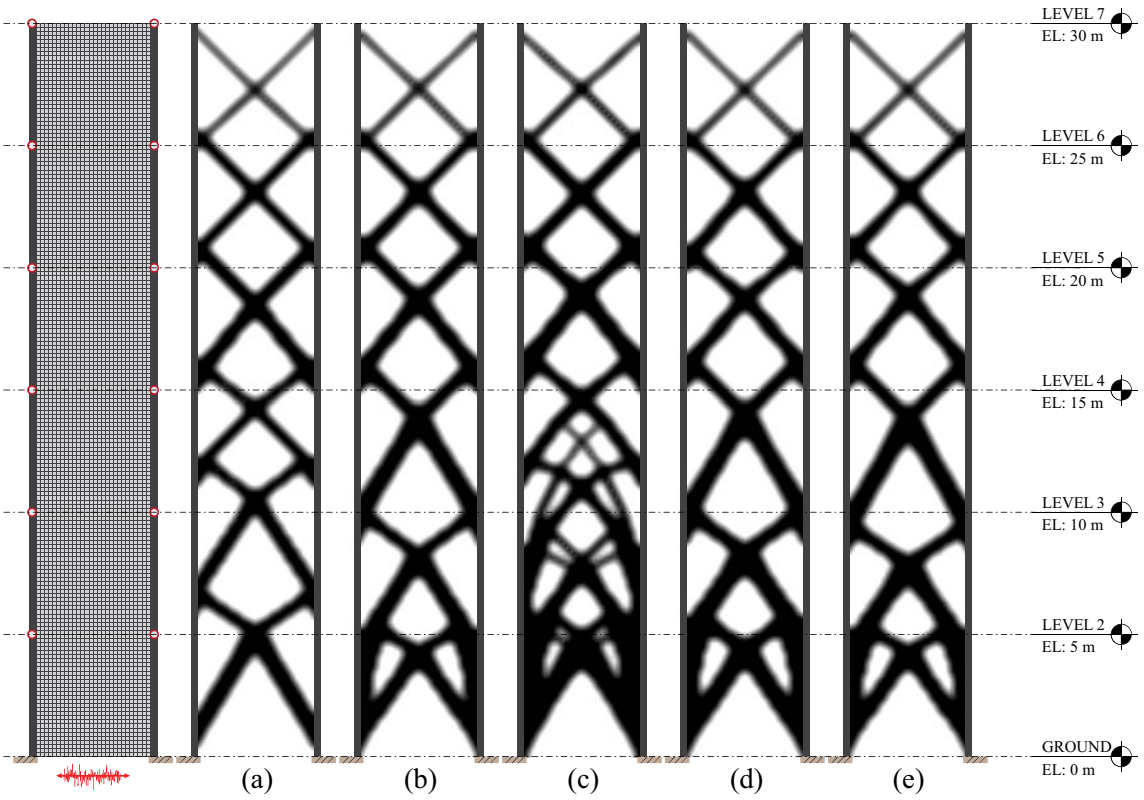

Fig. 22 Topology optimization solutions to the six-story building (Φ_0=2, β^{target}=2.5): (**a**) ω_f=4.7π, ζ_f=0.4; (**b**) ω_f=5.0π, ζ_f=0.4; (**c**) ω_f=5.3π, ζ_f=0.4; (**d**) ω_f=5.0π, ζ_f=0.2; (**e**) ω_f=5.0π, ζ_f=0.3

β^{target}=2.0. The different number of pattern repetition constraints in topology optimization result in various material distributions so that those can be implemented into aesthetical facades design with structural engineering. The convergence histories of solutions over iterative procedure of the optimization are shown in Fig. 26.

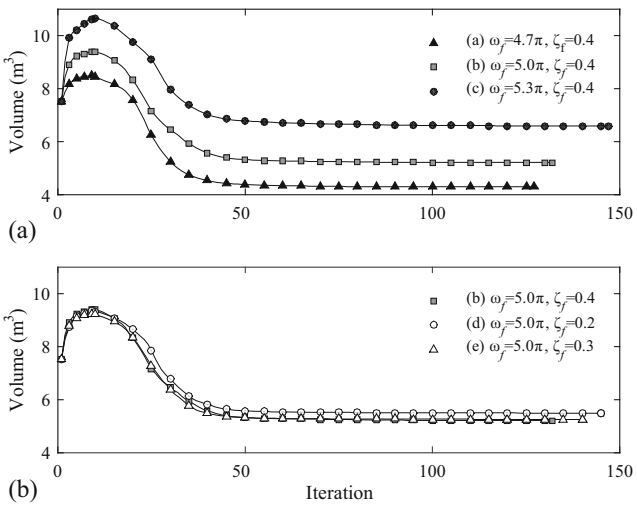

Fig. 23 Convergence history of topology optimization solutions shown in Fig. 22 (Φ_0=2, β^{target}=2.5). (**a**) change in the predominant frequency of the random process; (**b**) change in the bandwidth of the random process

6 Concluding remarks

In this paper, a new topology optimization framework is proposed for structures under stochastic excitations. For the linear structure subjected to the Gaussian excitation, the instantaneous failure probability regarding stochastic response is obtained from the closed form solution by using the discrete representation method. A formulation of the adjoint method is created to evaluate the sensitivities of the instantaneous failure probability described by the discrete representation method. The proposed stochastic topology optimization method and sensitivity formulations are applied to numerical examples for optimizing lateral bracing systems under stochastic ground motions. In the first numerical example, effects of varying model parameters and prescribed probabilistic values, such as column size, intensities of Gaussian white process, thresholds and reliability indices are studied. By investigating the failure probabilities of optimization solutions at different time points, it is also shown that the instantaneous failure probability can be a

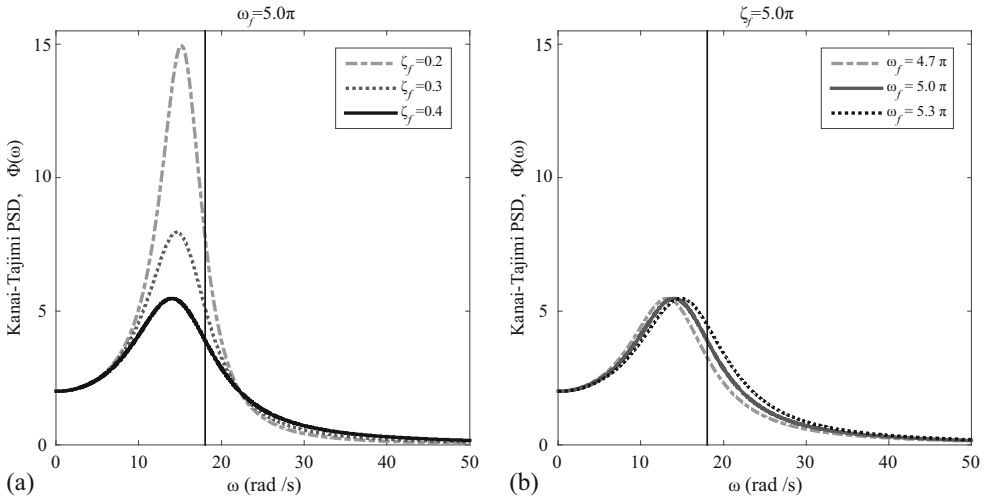

Fig. 24 Power spectral density of ground excitations (Φ_0=2) while changing (**a**) damping ratios and (**b**) predominant frequencies

reasonable indicator of the entire process if the probability is evaluated after stationarity is achieved. In addition, studies on changes in structural responses of topology optimization solutions considering the standard density method (with gray region) and the interpreted discrete solutions (i.e. black and white) show that the latter (discrete) shows reduced overall response with respect to the former, which indicates lower failure probability. Effects of ground motion characteristics such as the predominant frequency and the damping ratio of the Kanai-Tajimi filter model on final topologies are investigated in the second example. In summary, the proposed topology optimization method can provide structural engineers with an efficient and accurate method to

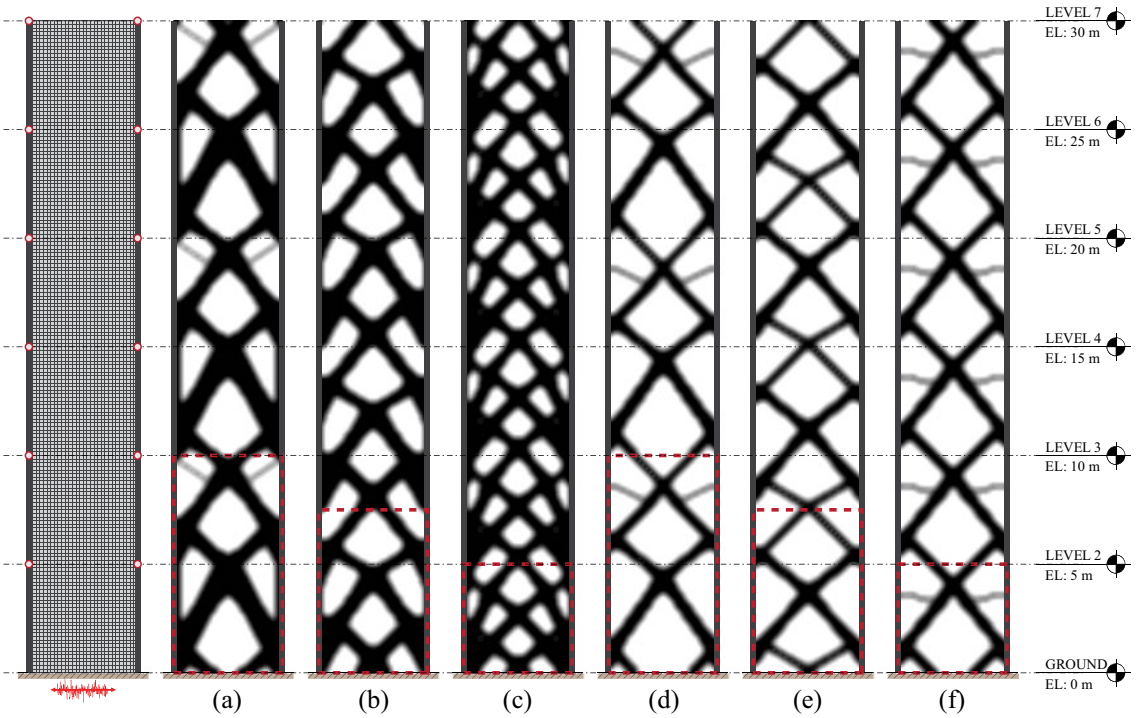

Fig. 25 Topology optimization solutions to the six-story building example with the pattern repetition constraint (Φ_0=2, ω_f=5.0π, ζ_f=0.4): (**a**) m=3, β^{target}=2.5; (**b**) m=4, β^{target}=2.5; (**c**) m=6, β^{target}=2.5; (**d**) m=3, β^{target}=2.0; (**e**) m=4, β^{target}=2.0; (**f**) m=6, β^{target}=2.0

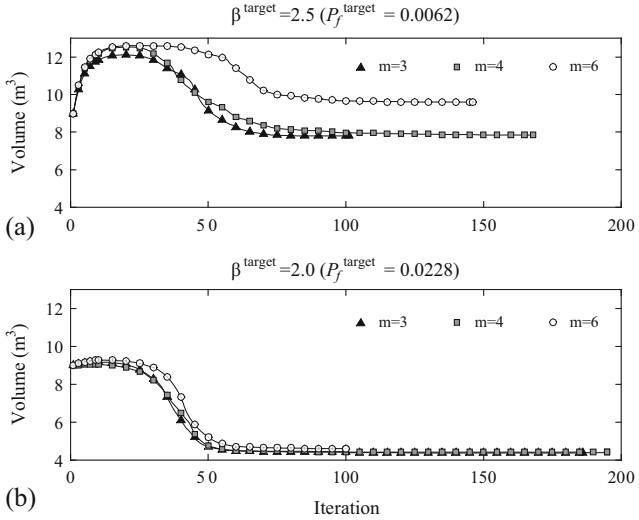

Fig.26 Convergence history of topology optimization solutions shown in Fig. 25 (Φ_0=2, ω_f=5.0π, ζ_f=0.4): (**a**) target reliability index β^{target}= 2.5; (**b**) target reliability index β^{target}=2.0

obtain optimal topologies while satisfying probabilistic constraints defined in terms of instantaneous failure probability under stochastic input excitations. When the stochastic response of a structure is non-Gaussian due to either non-linear system or non-Gaussian input excitations, the framework proposed in this paper is able to compute the failure probability efficiently by utilizing structural reliability methods such as FORM or SORM, instead of using the closed-form solution described in this paper. Furthermore, the proposed method can be extended to system reliability problems to incorporate the first-passage probability, multiple checkpoint locations in a structure or multiple failure modes into topology optimization under stochastic excitations. That extension will require evaluating multiple failure events at discretize time points and locations using on an efficient structural reliability analysis. In addition, a sensitivity analysis needs to be altered for the extension based on the proposed sensitivity approach in this paper.

Acknowledgements The authors gratefully acknowledge funding provided by the National Science Foundation (NSF) through project CMMI 1234243. We also acknowledge support from the Raymond Allen Jones Chair at the Georgia Institute of Technology. The second author also acknowledges the support from the Integrated Research Institute of Construction and Environmental Engineering at Seoul National University, and the National Research Foundation of Korea (NRF) Grant (No. 2015R1A5A7037372), funded by the Korean Government (MSIP). Any opinion, finding, conclusions or recommendations expressed here are those of the authors and do not necessarily reflect the views of the sponsors.

Appendix: Derivation of (11)

To derive (11) with a uniform time step, the convolution integral in (9) is carried out for discrete time intervals. An entry of the vector $\mathbf{a}(t_j)$ can be written as follows:

$$a_i(t_j) = \int_0^{t_j} s_i(\tau) h_s(t_j - \tau) d\tau \tag{A.1}$$

where

$$t_i = i\Delta t,\ t_j = j\Delta t \tag{A.2}$$

Then, one can consider the following three cases:

Case 1: $i=j$

$$\begin{aligned} a_i(t_i) &= \int_0^{t_i} \sqrt{2\pi\Phi_0\Delta t}\cdot h_f(\tau - t_i) h_s(t_i - \tau) d\tau \\ &= \sqrt{2\pi\Phi_0\Delta t}\cdot \left(\int h_f(\tau - t_i) h_s(t_i - \tau) d\tau \right)\Big|_{\tau = t_i} \\ &\left(\because h_f(\tau - t_i) = 0 \text{ for } 0 \le \tau < t_i\right) \end{aligned} \tag{A.3}$$

Case 2: $i>j$

$$\begin{aligned} a_i(t_j) &= \int_0^{t_j} \sqrt{2\pi\Phi_0\Delta t}\cdot h_f(\tau - t_i) h_s(t_j - \tau) d\tau \\ &= 0 \left(\because h_f(\tau - t_i) = 0 \text{ for } 0 \le \tau < t_i\right) \end{aligned} \tag{A.4}$$

Case 3: $i<j$

$$\begin{aligned} a_i(t_j) &= \int_0^{t_j} \sqrt{2\pi\Phi_0\Delta t}\cdot h_f(\tau - t_i) h_s(t_j - \tau) d\tau \\ &= \int_{t_i}^{t_j} \sqrt{2\pi\Phi_0\Delta t}\cdot h_f(\tau - t_i) h_s(t_j - \tau) d\tau \\ &\left(\because h_f(\tau - t_i) = 0 \text{ for } 0 \le \tau < t_i\right) \\ &= \int_0^{t_j - t_i} \sqrt{2\pi\Phi_0\Delta t}\cdot h_f(\tilde{\tau}) h_s(t_j - t_i - \tilde{\tau}) d\tilde{\tau} \\ &= \int_0^{c\Delta t} \sqrt{2\pi\Phi_0\Delta t}\cdot h_f(\tilde{\tau}) h_s(c\Delta t - \tilde{\tau}) d\tilde{\tau},\ c = j - i \end{aligned} \tag{A.5}$$

Thus,

$$\begin{aligned} a_i(t_j) &= a_i(j\Delta t) \\ &= \begin{cases} a_n(t_n) & i = j \\ 0 & i > j \\ a_{n-c}(t_n) & i < j,\ c = j - i \end{cases} \end{aligned} \tag{A.6}$$

Therefore, the uniform step size (t_n-t_{n-1}=Δt, t_n=t_0) in the convolution integral leads to the following expression:

$$a_i(t_j) = a_i(j\Delta t) = a_{n+i-j}(t_0),\ \ i = 1, 2, \ldots, n,\quad j = i, \ldots, n \tag{A.7}$$

References

Allen M, Raulli M, Maute K, Frangopol DM (2004) Reliability-based analysis and design optimization of electrostatically actuated MEMS. Comp Struc 82(13–14):1007–1020

Almeida SRM, Paulino GH, Silva ECN (2010) Material gradation and layout in topology optimization of functionally graded structures: a global–local approach. Struct Multidiscip Optim 42(6):855–868

ASCE. (2010). Minimum design loads for buildings and other structures. ASCE 7–10, Reston, VA

Bendsøe MP (1989) Optimal shape design as a material distribution problem. Struct Multidiscip Optim 1(4):193–202

Bendsøe MP, Kikuchi N (1988) Generating optimal topologies in structural design using a homogenization method. Comput Methods Appl Mech Eng 71:197–224

Bendsøe MP, Sigmund O (1999) Material interpolation schemes in topology optimization. Arch Appl Mech 69(9):635–654

Bendsøe MP, Sigmund O (2003) Topology optimization – theory, methods and applications. Springer Verlag, New York

Bourdin B (2001) Filters in topology optimization. Int J Numer Methods Eng 50(9):2143–2158

Chan SP, Cox HL, Benfield WA (1962) Transient analysis of forced vibrations of complex structural mechanical systems. J R Aeronaut Sot 66:457–460

Chen X, Kareem A (2005) POD-based modeling, analysis, and simulation of dynamic wind load effects on structures. J Eng Mech 131(4): 325–339

Chen L, Letchford CW (2005) Proper orthogonal decomposition of two vertical profiles of full-scale nonstationary downburst wind speeds[lzcl]. J Wind Eng Ind Aerodyn 93(3):187–216

Chen S, Chen W, Lee S (2010) Level set based robust shape and topology optimization under random field uncertainties. Struct Multidiscip Optim 41(4):507–524

Choi K, Kim N (2005) Structural sensitivity analysis and optimization 1. Springer-Verlag, New York

Clough R, Penzien J (1993) Dynamics of structures. McGraw Hill, New York

Deodatis G, Shinozuka M (1988) Autoregressive model for nonstationary stochastic processes. J Eng Mech 114(11):1995–2012

Der Kiureghian A (2000) The geometry of random vibrations and solutions by FORM and SORM. Probabilistic Eng Mech 15:81–90

Der Kiureghian A (2004) First- and second-order reliability methods. In: Nikolaidis E, Ghiocel DM, Singhal S (eds) Engineering Design Reliability Handbook. CRC Press, Boca Raton, FL, **Chap. 14**

Diaz AR, Kikuchi N (1992) Solutions to shape and topology eigenvalue optimization problems using a homogenization method. Int J Numer Methods Eng 35:1487–1502

Diaz AR, Sigmund O (1995) Checkerboard patterns in layout optimization. Struc Optim 10:40–45

Du J, Olhoff N (2007) Topological design of freely vibrating continuum structures for maximum values of simple and multiple eigenfrequencies and frequency gaps. Struct Multidiscip Optim 34: 91–110

Fujimura K, Der Kiureghian A (2007) Tail-equivalent linearization method for nonlinear random vibration. Probabilistic Eng Mech 22(1): 63–76

Gersch W, Yonemoto J (1977) Synthesis of multivariate random vibration systems: A two-stage least squares ARMA model approach. J Sound Vib 52(4):553–565

Grigoriu M (1993) On the spectral representation method in simulation. Probabilistic Eng Mech 8(2):75–90

Grigoriu M (2003) Algorithm for generating sampling of homogeneous Gaussian fields. J Eng Mech 129(1):43–49

Guest JK, Igusa T (2008) Structural optimization under uncertain loads and nodal locations. Comput Methods Appl Mech Eng 198(1):116–124

Guest JK, Prevost JH, Belytschko T (2004) Achieving minimum length scale in topology optimization using nodal design variables and projection functions. Int J Numer Methods Eng 61(2):238–254

Haftka RT, Gürdal Z (1992) Elements of structural optimization. 3rd edition, Springer

Haug E, Arora S (1978) Design sensitivity analysis of elastic mechanical systems. Comput Methods Appl Mech Eng 15(1):35–62

Haug J, Choi K, Komkov V (1986) Design sensitivity analysis of structural systems. Academic press, Orlando FL Allen M, Raulli M, Maute K, Frangopol, DM (2004) Reliability-based analysis and design optimization of electrostatically actuated MEMS. Computer & Structures, 82(13–14):1007–1020

Houbolt JC (1950) A recurrence matrix solution for the dynamic response of elastic aircraft. J Aeronaut Sci 17(9):540–550

Hulbert GM, Chung J (1996) Explicit time integration algorithms for structural dynamics with optimal numerical dissipation. Comput Methods Appl Mech Eng 137(2):175–188

Jalalpour M, Guest JK, Igusa T (2013) Reliability-based topology optimization of trusses with stochastic stiffness. Struct Saf 43:41–49

Jensen JS, Pedersen NL (2006) On maximal eigenfrequency separation in two-material structures: the 1D and 2D scalar cases. J Sound Vib 289(4–5):967–986

Jog CS, Haber RB (1996) Stability of finite element models for distributed-parameter optimization and topology design. Comput Methods Appl Mech Eng 130:203–226

Kang J, Kim C, Wang S (2004) Reliability-based topology optimization for electromagnetic systems. COMPEL: Int J Comput Math Elec Electron Eng 23(3):715–723

Kharmanda G, Olhoff N, Mohamed A, Lemaire M (2004) Reliability-based topology optimization. Struct Multidiscip Optim 26(5):295–307

Kim YY, Yoon GH (2000) Multi-resolution multi-scale topology optimization–a new paradigm. Int J Solids Struct 37:5529–5559

Kim C, Wang S, Rae K, Moon H, Choi KK (2006) Reliability-based topology optimization with uncertainties. J Mech Sci Technol 20(4):494–504

Kitagawa G (1996) Monte Carlo filter and smoother for non-Gaussian nonlinear state space models. J Comput Graph Stat 5(1):1–25

Kohn RV, Strang G (1986) Optimal design and relaxation of variational problems. Comm Pure Appl Math 39:113–137, **139–182, 353–377**

Konakli K, Der Kiureghian A (2012) Simulation of spatially varying ground motions including incoherence, wave-passage and differential site-response effects. Earthq Eng Struct Dyn 41(3):495–513

Li CC, Der Kiureghian A (1993) Optimal discretization of random fields. J Eng Mech 119(6):1136–1154

Liu J, Chen R (1998) Sequential Monte Carlo methods for dynamic systems. J Am Stat Assoc 93(443):1032–1044

Lógó J, Ghaemi M, Rad MM (2009) Optimal topologies in case of probabilistic loading: the influence of load correlation. Mech Based Design Struc Mach 37(3):327–348

Luo Y, Kang Z, Luo Z, Li A (2009) Continuum topology optimization with non-probabilistic reliability constraints based on multi-ellipsoid convex model. Struct Multidiscip Optim 39(3):297–310

Lutes LD, Sarkani S (2003) Random vibrations: analysis of structural and mechanical systems. Elsevier Butterworth-Heinemann, Burlington MA

Ma ZD, Cheng HC, Kikuchi N (1994) Structural design for obtaining desired eigenfrequencies by using the topology and shape optimization method. Comput Syst Eng 5(1):77–89

Ma ZD, Kikuchi N, Cheng HC (1995) Topological design for vibrating structures. Comput Methods Appl Mech Eng 121(1–4):259–280

Maeda Y, Nishiwaki S, Izui K, Yoshimura M, Matsui K, Terada K (2006) Structural topology optimization of vibrating structures with

specified eigenfrequencies and eigenmode shapes. Int J Numer Methods Eng 67:597–628

Maute K, Frangopol DM (2003) Reliability-based design of MEMS mechanisms by topology optimization. Comp Struct 81(8–11): 813–824

Mignolet MP, Spanos PD (1987) Recursive simulation of stationary multivariate random processes-Part I. J Appl Mech 54(3):674–680

Min S, Kikuchi N, Park YC, Kim S, Chang S (1999) Optimal topology design of structures under dynamic loads. Struct Multidiscip Optim 17(2–3):208–218

NEHRP (2009) Recommended seismic provisions for new buildings and other structures (FEMA P-750). Federal Emergency Management Agency, Washington, D. C

Newmark NM (1959) A method of computation for structural dynamics. J Eng Mech 85:67–94

Nguyen TH, Song J, Paulino GH (2011) Single-loop system reliability-based topology optimization considering statistical dependence between limit-states. Struct Multidiscip Optim 44(5):593–611

Novak D, Stoyanoff S, Herda H (1995) Error assessment for wind histories generated by autoregressive method. Struct Saf 17(2):79–90

Pedersen NL (2000) Maximization of eigenvalues using topology optimization. Struct Multidiscip Optim 20:2–11

Poulsen A (2002) Topology optimization in wavelet space. Int J Numer Methods Eng 53:567–582

Rezaeian S, Der Kiureghian A (2008) A stochastic ground motion model with separable temporal and spectral nonstationarities. Earthq Eng Struc Dyn 37(13):1565–1584

Rezaeian S, Der Kiureghian A (2010) Simulation of synthetic ground motions for specified earthquake and site characteristics. Earthq Eng Struc Dyn 39(10):1155–1180

Rezaeian S, Der Kiureghian A (2012) Simulation of orthogonal horizontal ground motion components for specified earthquake and site characteristics. Earthq Eng Struc Dyn 41(2):335–353

Rozvany GIN (2008) Exact analytical solutions for benchmark problems in probabilistic topology optimization. In: EngOpt 2008–international conference on engineering optimization, Rio de Janeiro

Rozvany GIN, Zhou M, Birker T (1992) Generalized shape optimization without homogenization. Struct Multidiscip Optim 4(34):250–252

Rubio WM, Paulino GH, Silva ECN (2011) Tailoring vibration mode shapes using topology optimization and functionally graded material concepts. Smart Mater Struct 20(2):025009

Shinozuka M (1972) Monte Carlo solution of structural dynamics. Comp Struc 2(5–6):855–874

Shinozuka M, Deodatis G (1991) Simulation of the stochastic process by spectral representation. Appl Mech Rev 44(4):29–53

Shinozuka M, Deodatis G (1996) Simulation of multi-dimensional Gaussian stochastic fields by spectral representation. Appl Mech Rev 49(1):29–53

Shinozuka M, Jan CM (1972) Digital simulation of random processes and its applications. J Sound Vib 25(1):111–128

Sigmund O (2007) Morphology-based black and white filters for topology optimization. Struct Multidiscip Optim 33(4–5):401–424

Sigmund O, Petersson J (1998) Numerical instabilities in topology optimization: a survey on procedures dealing with checkerboards, mesh-dependencies and local minima. Struc Optimization 16(1):68–75

Song J, Kang WH (2009) System reliability and sensitivity under statistical dependence by matrix-based system reliability method. Struct Saf 31(2):148–156

Spanos PD, Ghanem R (1989) Stochastic finite element expansion for random media. J Eng Mech 115(5):1035–1053

Spanos PD, Mignolet MP (1987) Recursive simulation of stationary multivariate random processes–Part II. J Appl Mech 54(3):681–687

Spanos PD, Mignolet MP (1990) Simulation of Stationary Random Processes: Two-Stage MA to ARMA Approach. J Eng Mech 116(3):620–641

Stromberg LL, Beghini A, Baker WF, Paulino GH (2011) Application of layout and topology optimization using pattern gradation for the conceptual design of buildings. Struct Multidiscip Optim 43(2): 165–180

Svanberg K (1987) The method of moving asymptotes - a new method for structural optimization. Int J Numer Methods Eng 24(2):359–373

Zhang J, Ellingwood B (1994) Orthogonal series expansions of random fields in reliability analysis. J Eng Mech 120(12):2660–2677

Zienkiewicz OC (1977) A new look at the newmark, houbolt and other time stepping formulas. A weighted residual approach. Earthq Eng Struc Dyn 5(4):413–418